



Research article

Improving the binding affinity of plastic degrading cutinase with polyethylene terephthalate (PET) and polyurethane (PU); an in-silico study

Deves Sabari V L^a, Gokulnath Rajmohan^a, Roshine S B^a, Srivaishnavi S^a, Kishore Nagasubramanian^a, Senthil Kumar G^a, Ponnusami Venkatachalam^{b,*}

^a School of Chemical & Biotechnology, SASTRA Deemed to be University, Thanjavur, Tamil Nadu, India

^b Biomass Conversion and Bioproducts Laboratory, Center for Bioenergy, School of Chemical & Biotechnology, SASTRA Deemed University, Thirumalaisamudram, Tamil Nadu, India

ARTICLE INFO

Keywords:

Cutinase
Enzymatic Plastic degradation
Molecular docking
Molecular dynamic simulation

ABSTRACT

Plastic pollution is a worrying problem, and its degradation is a laborious process. Although enzymatic plastic breakdown is a sustainable method, drawbacks such as numerous plastic kinds of waste make the degradation challenging. Therefore, a multi-plastic degrading (MPD) enzyme becomes necessary. In this *in-silico* study, microorganisms and their enzymes that are known to degrade plastic polymers such as PET, PU, PVC, and PE were identified to assess their MPD capability. The cutinase of *Thermobifida fusca* was found to degrade both PET and PU polymers. The crystallized structure of cutinase was retrieved from PDB, and PET, PU ligands were docked using Schrodinger. However, the interactions between cutinase and the ligands were not efficient, as evidenced by the docking scores of -4.047 and -4.993 for PET and PU, respectively. Nevertheless, the interaction of the cutinase's active site with the ligands by hydrogen bond formation was promising. In this work, unconserved regions of cutinase were identified as potential mutation sites to enhance binding efficiency. *In-silico* Alanine Scanning Mutagenesis (ASM) and Site Saturation Mutagenesis (SSM) were performed as screening tests to find variants of cutinase with better docking scores for both ligands, specifically S136D, N28M, and S136Q. Molecular Dynamic Simulation (MDS) was performed for Wild Type (WT) cutinase, variants, and their respective complexes formed with the ligands. This simulation indicated the compactness, stability, and minimal energy of the variant complexes compared to WT complexes. Subsequent *in vitro* studies can ensure the improved degradation of both PET and PU by the variants.

1. Introduction

Plastics have become an integral part of our lives due to their favourable qualities, such as affordability, resilience to weathering, lightweight nature, transparency, and durability, which have led to a long-term rise in their consumption [1]. The global polymer market exceeds 500 million metric tonnes (Mt) annually. This includes about 80 million Mt of man-made fibers, 30 million Mt of rubber goods, and roughly 23 million Mt and 370 million Mt of structural and functional polymers, respectively. The amount of plastic

* Corresponding author.

E-mail address: vponnu@chem.sastra.edu (P. Venkatachalam).

produced has increased globally by about 35 % in the last ten years, and it is predicted to reach 700 million Mt by 2030 [2], and 1.1 billion Mt by 2050 [3]. The most produced plastics are Polyethylene (PE), Polyethylene terephthalate (PET), Polyvinyl Chloride (PVC), and Polyurethane (PU), with annual production of about 99.6 million Mt, 73.39 million Mt, 44.3 million Mt, and 16.9 million Mt, respectively ([4]a). Owing to their remarkable thermal and mechanical qualities, PE exhibits a greater capacity to resist corrosion and environmental deterioration [5]. PET is used for various applications such as packaging, textiles, and engineering plastics [6]. PVC has wide utility in agriculture, electronics, and construction [7,8]. PU (organic units of carbamate linkages: polyols and polyisocyanates) is used to make footwear, car seats, furniture, and refrigerator insulation [9–11].

However, the burden of managing plastic waste has also increased as production increases. The current plastic management system is inadequate, and the recyclability is only about 9 % of the garbage produced, which is a negligible percentage compared to the entire plastic production. It is estimated that 80 % of the waste produced ends up in landfills or the environment [12]. Mechanical recycling is a common strategy but has its own limitations, such as high expense, deterioration of mechanical properties [13], and varying composition of plastics which might result in the non-isotropic nature of the product [14]. This is because people do not dispose of the plastics according to their type; instead dump them together with non-biodegradable wastes [15]. In addition, the COVID-19 pandemic has further complicated the management of plastic pollution by producing more amounts of medical plastic waste and a lack of attention to plastic waste management was prevalent during that period [16].

Therefore, effective plastic waste management is crucial for sustainability and environmental protection. Enzymes are considered highly effective biocatalysts because of their ability to operate under milder conditions (e.g., temperature, pH, and pressure), their high degree of selectivity, and their low environmental impact including lower energy consumption and waste generation[17]. It has been found that some microbes produce enzymes capable of breaking down these plastics. These enzymes facilitate the primary degradation of the polymer chains by breaking them down and enabling the absorption within the cell, releasing them as metabolic products such as CO₂, H₂O, CH₄, and N₂ [18]. The majority of these enzymes are members of the hydrolase class (EC 3), which also includes lipases, depolymerases, esterases, and PETases [19], and are known to hydrolyze several commonly used plastics by cleaving their long carbon backbone ([4]b).

Findings have shown that a detailed understanding of the enzyme structure that breaks long carbon chains would facilitate the advancement of plastic waste management in the future. A PET degrading enzyme produced by the marine bacterium *Pseudomonas aestusnigri* showed increased PET degradation after introducing mutation at Y250S in the crystal structure of polyester hydrolase [20]. Another study used *Ideonella sakaiensis* to degrade the PET by introducing the mutations (site-directed mutagenesis) at S93M, W159F, and N241F of PETase [21]. Notably, aforementioned enzymes exhibit α- and β-hydrolase protein scaffolds. In addition to these results, the affinity of the natural and mutated plastic degrading enzymes for their respective plastic substrates has been shown to be a critical factor in plastic degradation process [22]. Thus, there must be strong structural correlations between protein structure and its activity. Moreover, protein engineering should be applied to improve the activity, ability, and binding affinity of plastic-degrading enzymes in the future of plastic waste management.

However, traditional research strategies minimize the identification of the best enzymes, organisms, and their engineered versions due to their ability to expedite the time, labor, and cost in the development of innovative enzymes [23]. The recent advancements in *in silico* techniques have garnered a great deal of interest [24], including the prediction of a compound's structure by high-throughput screening [25]. These techniques are widely accepted and practised in the medicinal fields and could potentially reveal details about the unidentified molecular structures, such as enzymes and possible ligands for them [26]. Moreover, similar approaches have already been adopted by Enyoh et al. [27] to screen the enzymes and their diverse binding affinities with different plastics. They found that the manganese peroxidase from *Phanerochaete chrysosporium* showed a better affinity than other comparative plastic degradable enzymes. Protein adsorption and interaction at material interfaces is key concept that builds the computational approach to study protein-plastic interaction [28]. The study focuses on the difficulties of protein interactions with non-biological surfaces such as plastic. Recognizing these constraints emphasizes the need for computational techniques in situations when experimental data is restricted, which justifies the use of docking scores to investigate protein-plastic interactions [29]. The findings of Schottler et al. [30] back up docking techniques in non-traditional biological systems, revealing the adaptability and usefulness of computational predictions for analyzing protein-plastic interactions. In particular, arginine, leucine, and serine of manganese peroxidase are shown to be the essential residues that showed strong interactions with all selected plastics via van der Waals forces, conventional hydrogen bonding, carbon-hydrogen bond, and Pi-Pi Interactions (Enyoh et al., 2022b).

Despite the study stating the importance of binding affinity, they lack in showing the improvements in affinity by mutations. Our major goal is to improve the binding affinity of cutinase from *Thermobifida fusca* to PET and PU substrates by targeted modifications. We also want to boost the enzyme's catalytic performance by discovering mutations that strengthen its interaction with substrate molecules, leading to faster plastic degradation. The precise targets were chosen to enhance the enzyme's efficacy in breaking down several forms of plastic, addressing the issue of mixed plastic waste in environmental applications.

The objectives include (i) identification a multi-plastic degrading enzyme (MPD), (ii) improving the binding affinity of the chosen enzyme towards selected plastic ligands (PET and PU) using *in-silico* techniques, (iii) mutating it in the unconserved regions by applying site saturation mutagenesis to find the best potential sites and (iv) assessing the binding affinity of the mutants with the plastic ligands using molecular docking and molecular dynamics simulations.

2. Materials and methods

2.1. Enzyme selection and sequence alignment

We selected enzymes capable of degrading four major types of plastics: PET, PVC, PU, and PE. This selection was based on previous literature reports that enzymatic degradation of multiple plastics. Compared to other PET-degrading enzymes, *T. fusca* cutinase has exhibited the ability to degrade many plastics, exceptional catalytic efficiency, and stability making it a suitable choice for dealing with various forms of plastic waste. Furthermore, the enzyme's moderate thermal stability and responsiveness to mutations make it ideal for computational optimization to improve binding affinity and catalytic activity. We believe that these properties make *T. fusca* cutinase a useful model for creating strong plastic-degrading enzymes. Enzyme sequences were retrieved in FASTA format from UniProt [31] and aligned using Clustal Omega to identify homologous enzymes [32].

2.2. Ligand selection and identification of binding pockets

Plastics potentially targeted by MPD enzymes were considered as ligands. Dimer structures of these substrates were generated using the 2D sketcher in Schrodinger Maestro Version 12.3.013 and saved in.pdb format for further analysis. The 3D structure of the MPD enzyme was used to identify binding pockets using the CASTp (Computer Atlas of Surface Topography of Proteins, v 3.0) server [33].

2.3. Selection of unconserved regions and mutagenesis

Mutations in unconserved residues are known to cause functional divergence in the enzymes, which may either improve or reduce enzyme activity [34]. These residues were identified through Multiple Sequence Alignment (MSA) of homologous of the MPD enzyme, which were obtained by Protein BLAST, and visualized using Jalview, an online platform for sequence analysis. Jalview facilitates visualization and editing of sequences, construction of phylogenetic trees, and principal compound analysis (PCA) [35]. The unconserved regions of MPD enzyme were mutated to alanine due to its propensity to form alpha helices and beta sheets. Alanine is an accepted single residue for mutational scanning because it retains the beta carbon and does not change the conformation of the protein [36]. ASM was performed in the Schrodinger Maestro Version 12.3.013 as a primary screening test.

The residues screened in the above analysis underwent Site Saturation Mutagenesis (SSM). Alanine was replaced by the remaining 18 amino acids, providing variants of the MPD enzyme. The docking procedure was performed in a similar manner. By choosing the residues with the highest docking scores, top three most promising candidates for Molecular Dynamic Simulation were identified. Thus, it served as the secondary screening test.

2.4. Molecular docking

Docking is a computational approach for studying interactions between proteins and synthetic polymers such as plastics. Molecular docking helps to determine binding types, affinities and interaction processes in non-traditional biological systems. While acknowledging its limitations, the work suggests that combining docking with complementary approaches can provide precise insights into protein-plastic interactions [37]. All the molecular docking studies were performed using the Glide module in Schrodinger Maestro Version 12.3.013. The OPLS3e force field was applied uniformly with a neutral pH of 7 ± 0.2 . The heteroatoms and solvent water molecules in the apoenzyme were removed. An efficient extra precision (XP) platform was used for all the docking functions performed.

2.5. Molecular dynamics simulation

2.5.1. Simulation of native protein

To gain insights into the molecular stability of the MPD enzyme, we conducted simulations of its three-dimensional structure using the OPLS all-atom force field. This approach enabled more accurate conformational analysis and improved understanding of binding free energies. Simulations were performed using GROMACS v5.0.2.

The water-free protein.pdb file was converted to GROMACS file (.gro), generating topology, position restraint, and post-processed structure files. We employed the OPLS all-atom force field for optimal force field selection. The protein was placed in a cube with dimension 1.5 nm. The charge of the protein was neutralized by the addition of sodium ions. The protein minimization was achieved using the steepest decent algorithm of the conjugate gradient method.

To assess positional stability, the protein was subjected to energy minimization and equilibration under NVT (constant number of particles, volume, and temperature) & NPT (constant number of particles, pressure, and temperature) ensembles for 100 ps. Water molecule geometry and bond angle constraints were applied using the SETTLE and LINCS algorithms. SETTLE is a constraint technique intended for stiff water molecules that is widely used in molecular dynamics simulations. It guarantees that the binding lengths and angles in water molecules remain constant which can considerably speed up simulations by allowing for bigger time steps [38]. The LINCS (Linear Constraint Solver) technique applies bond constraints in molecular dynamics. It is especially effective for big, complicated biomolecules and avoids the iterative technique employed by SHAKE, lowering processing costs. LINCS is well-known for its resilience and stability, particularly, in systems with numerous bonds [39]. The system temperature was maintained at 300 K using V-rescale, a method that rescales velocities to regulate temperature. This approach ensures stable dynamics and consistent thermostat

performance [40]. Pressure (1 atm) and volume were controlled anisotropically using Parrinello-Rahman algorithm constraint matrix. The Parrinello-Rahman technique is a popular barostat in molecular dynamics simulations for maintaining constant pressure. Unlike simpler pressure-coupling approaches, it permits anisotropic scaling of the simulation box, making it suited for complicated systems where the box's shape and volume might change. This barostat is very effective in systems involving phase transitions or extremely anisotropic materials [41]. This allowed for realistic fluctuations in system properties. The equilibrated system was subjected to simulation up to 100 ns. Simulation results were analysed using appropriate bioinformatics tools and data was recorded for further investigation.

2.5.2. Simulation of best docked complex

To gain insights into the molecular stability and dynamics of the protein-ligand complex, simulations were performed using GROMACS v5.0.2. The OPLS all-atom force field was chosen to accurately depict the interactions within the MPD_PET and MPD_PU complexes. Topology files for both the protein and ligands were generated, with the ligand topology generated using the LigParGen tool [42]. The protein-ligand complexes were then constrained within a cubic box with dimensions of 1.5 nm, and sodium ions were added to neutralize the system. Throughout the 100 ns molecular dynamics (MD) simulation, structural data were retrieved every 2 ps. The resulting trajectory data were saved and analysed using appropriate tools within the GROMACS package. Analysis included the calculation of Root Mean Square Deviation (RMSD), Root Mean Square Fluctuation (RMSF), Solvent Accessible Surface Area (SASA), hydrogen bond distribution and frequency, various GROMACS energies, Radius of Gyration (Rg), Principal Component Analysis (PCA), MM-PBSA (Molecular Mechanics/Poisson Boltzmann Surface Area), MM-GBSA (Molecular Mechanics/Generalized Born Surface Area), and Free Energy Landscapes (FEL).

2.6. PRODIGY

PROtein binDIIng enerGY (PRODIGY) prediction web service was used to verify the binding affinity of the protein-ligand complexes obtained for the MPD enzyme and its variants. The PRODIGY-LIGAND module was used to predict the binding affinities [43,44].

3. Results

3.1. Collection of enzymes

The list of enzymes chosen for this study is given in Table 1. The majority of the enzymes are of the hydrolase class. Laccase and cutinase are recognized for their plastic biodegradation potential. Cutinase, particularly from *T. fusca*, is a well-studied enzyme that can break down ester bonds in polyester-based plastics such as PET and PU. It has been engineered widely in previous studies, to improve its stability and efficiency to develop sustainable methods for recycling plastic waste. Their ability to degrade synthetic polymers makes them key players in the future of plastic waste management. ([20]; [45]; [46–58]).

Table 1
Microbial enzymes degrading PET, PE, PVC, and PU.

Enzyme	Organism	PDB id/Accession id	Reference
PET			
PETase	<i>Ideonella sakaiensis</i>	6ANE	[20]
Cutinase	<i>T. fusca</i>	4CG1	[50]
Lipase	<i>P. aestusnigri</i>	6SBN	[55]
Cutinase	<i>Fusarium solani pisi</i>	1CEX	[49]
Cutinase	<i>Humilica insolens</i>	4OYY	[49]
PE			
Manganese peroxidase	<i>Phanerochaete chrysosporium</i>	3M5Q	[48]
Unspecific peroxygenase	<i>Agrocybe aegerita</i>	2YOR	[52]
Lignin peroxidase	<i>Trametes cervine</i>	3Q3U	[58]
Laccase	<i>Trametes versicolor</i>	1KYA	[45]
Cutinase	<i>Fusarium solani</i>	1CUS	[45]
PVC			
Catalase	<i>Neurospora crassa</i>	1SY7	[57]
Dihydroxy-acid dehydratase	<i>Synechocystis sp. PCC 6803</i>	6NTE	[54]
Monooxygenase	<i>P. aeruginosa PAO1</i>	7SQX	Schmidt et a., 2017
Esterase	<i>P. aeruginosa</i>	3KVN	Schmidt et a., 2017
Laccase	<i>Trametes versicolor</i>	1GYC	[56]
PU			
Cutinase	Leaf compost metagenome	4EB0	[47]
Cutinase	<i>T. fusca</i>	4CG1	[47]
Lipase	<i>T. curvata DSM43183</i>	ACY95991.1	[59]
Amidase	<i>Rhodococcus erythropolis CCM2595</i>	AGT90042.1	[60]
Enantioselective amidase	<i>Agrobacterium tumefaciens</i>	Q9AHE8	[60]

3.2. Multiple sequence alignment and protein structure

The cutinase (PDB ID: 4CG1) from *T. fusca* was found to be an MPD enzyme, as it has been shown to degrade both PET and PU in independent studies. This is further supported by the percent identity matrix, which reveals 100 percent identity between 4CG1 and Q6A014 sequences (Fig. 1). The secondary structures and crystal structure of the selected enzyme (PDB ID: 4CG1) retrieved from the Protein Data Bank (PDB) are shown in Fig. 2(a) and (b), respectively.

3.3. Ligands selection

The plastics PU and PET were found to be degraded by cutinase from *T. fusca* (Table 1). Thus, PU and PET were selected as ligands and their dimers were drawn (Fig. 2(c) and (d)). The chemical structures of the ligands were acquired from the literature based on which the structures were drawn [59,60].

3.4. Identification of ligand binding pockets

The ligand binding pocket residues were G59, Y60, T61, G62, S66, H129, S130, M131, W155, I178, H208, F209, and N212. Fig. 2(e) represents the 3D visualization of the pocket.

3.5. Selection of unconserved regions

The target protein (UniProt ID: Q6A0I4) homologous proteins were found by performing protein BLAST. Among the retrieved hits, the top five homologous enzymes were selected based on criteria including high percent identity, 100 % query coverage, and the lowest expected value (E value). The FASTA sequences of the target protein (Q6A0I4) and its best five homologous proteins were aligned and visualized in Jalview. Unconserved areas were identified by a multiple sequence alignment of several mutant variants of *T. fusca* cutinase. Sites with amino acid changes between these variants were termed unconserved because they suggest locations where mutations occurred without affecting the enzymes' natural activity. A conservation criterion was established so that any residue with less than 100 % identity across all aligned sequences was designated as unconserved. This method allows us to concentrate on areas where mutations are more likely to improve or alter enzyme function. It revealed the unconserved residues that are represented as white columns in Fig. 3. These residues were identified as the potential sites for the ASM and SSM. The potential site residue positions are 18, 28, 29, 32, 33, 35, 64, 67, 72, 87, 98, 105, 106, 114, 136, 165, 182, 186, and 194 (Fig. 3).

3.6. Molecular docking

3.6.1. Wild type protein

The docking of Wild Type Cutinase (WT) with ligands PET and PU dimers gave several insights into the interaction between them. The WT_PET complex showed hydrogen bond formation with residues Y60, K159, and W155. The first two interactions happen in the terminals of dimer, whereas the third interaction happens in the ester bond between the monomer subunits.

Similarly, WT_PU complex consists of hydrogen bond formation with T207, T183, H184, S130, and W155. Among these bonds, the last three showed binding affinity towards the carbonyl oxygen present in the ligand. These are evident in Fig. 4(a) and (b).

3.6.2. Alanine mutated proteins

Alanine-mutated proteins were docked with the PET and PU ligands. Screening was done by comparing the docking scores of mutated proteins to those of the wild type (Fig. 5). Nine promising candidates were identified for SSM.

3.6.3. Site saturation mutagenesis

The screened residues from the ASM were mutated to every other amino acid and docked with the PET and PU ligands, as discussed

Fig. 1. Percent identity matrix for the list of enzymes that are tabulated.

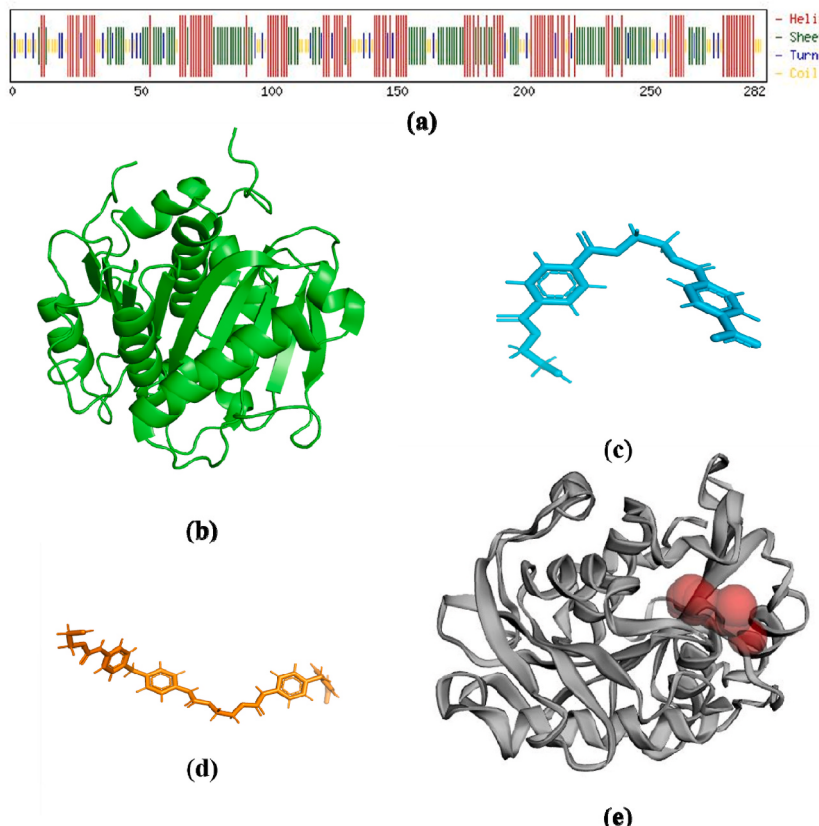


Fig. 2. Visualization of 4CG1_WT cutinase & ligand structures. (a) Secondary structure of 4CG1_WT cutinase. (b) Tertiary structure of 4CG1_WT cutinase (c) 3D structure of PET (d) 3D structure of PU (e) 3D structure of 4CG1_WT cutinase with the binding pockets (Area = 72.687 Å², Volume = 20.917 Å³) obtained using CASTp residues.

in section 2.3, to obtain the docking scores. The docking scores for each mutated variant are pictorially depicted in the heat map (Fig. 6 (a) for PET and Fig. 6 (b) for PU). Fig. 6 represents the gradients of the docking score resulting from positioning all the plausible mutations to the particular site, selected from the primary screening, into the secondary screening, which replaces the amino acid present in the mutated position with all possible amino acids. This is done to figure out which amino acid provides better binding ability to form the protein-ligand complex. The white mark is the docking score of wild type protein with the PET and PU. The idea is to get a lesser binding score for the variant than the wild type protein for both PET and PU. Thus, the figure represents a range of docking scores obtained, with blue ones being the desired result. All the combinations in blue have better docking scores than the wild type; among them, the combinations that managed to be blue in both PET and PU cases (S136D, N28M, and S136Q) were selected. Despite some variants showing better glide scores towards PET and PU separately, the objective of the research is to identify the top variants that show improved glide scores for both PET and PU ligands. Not much data is available in the literature for comparison docking scores for similar enzyme – plastic complexes. In a previous report, the docking scores for *T. fusca* cutinase – PU complex were reported to be –5.7 & –5.8 for 4CG1 & 4CG2, respectively [61]. The docking scores obtained in this study are more favourable compared to this previous report. Thus, the present simulation results suggest that we can achieve better degradation results through proposed mutations.

3.7. Molecular dynamics simulation

The dynamics of the protein-ligand interactions were examined using GROMACS simulation with 100 ns. The apoenzyme of wild type and mutated protein, along with ligands (PET and PU), were simulated. Root Mean Square Deviation (RMSD) and Root Mean Square Fluctuations (RMSF) were used to monitor the stability and structural changes of the complexes. Lesser RMSD indicates increased stability of complexes or proteins [62]. RMSF indicates the protein residue fluctuations. A higher RMSF of residues indicates greater mobility and suggests possible dynamic interactions within the complex in these regions, and a lower RMSF value indicates stable regions within the complex [63]. The maximum RMSD was observed around 0.3 nm for the variants and the minimum RMSD was shown by the wild type (4CG1_WT) cutinase structure. The 4CG1_WT_PET variant had notable fluctuation until 25 ns, after which the structure stabilized. Stability for the 4CG1_WT_PU complex was maintained throughout the simulation, although deviation was noted after 70 ns. 4CG1_S136D_PET structure showed better stability, yet deviation was perceived with two displacement peaks at 37.5

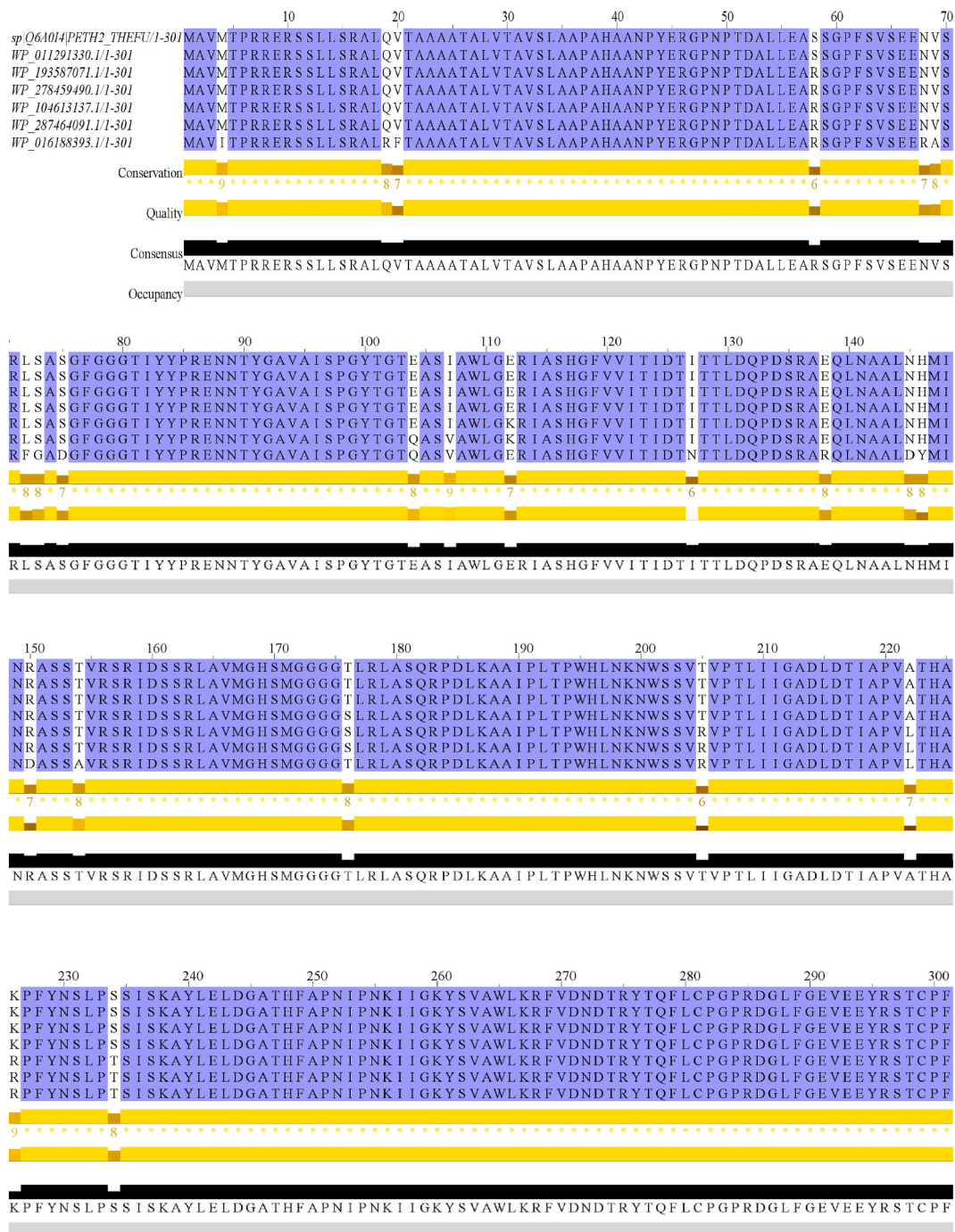


Fig. 3. The homologous proteins along with the cutinase [Q6A0I4] WT are viewed in Jalview, in which the white regions indicate the unconserved regions.

ns and 65 ns time points, respectively. Conversely, the 4CG1_S136D_PU complex exhibited minor fluctuations, with stability regained after 25 ns. Similarly, the RMSD data for the 4CG1_S136Q variant showed dynamic deviation initially until 40 ns, followed by stability with an RMSD of 0.22 nm. The 4CG1_S136Q_PET complex remained stable throughout the simulation, with the maximum deviation peak observed at 0.30 nm between 75 and 100 ns. Similarly, the 4CG1_S136Q_PU complex displayed dynamic behaviour, peaking at several time points such as 28 ns, 55 ns, 65 ns, and 90 ns, yet none of the peaks exceeded 0.23 nm. Overall, all 12 protein and complex structures remained stable in the selected environment, with RMSD values consistently below 0.30 nm (<0.50 nm). Notably, the 4CG1_N28M mutated protein and its ligand-bound complexes exhibited higher deviation from WT cutinase stability, particularly

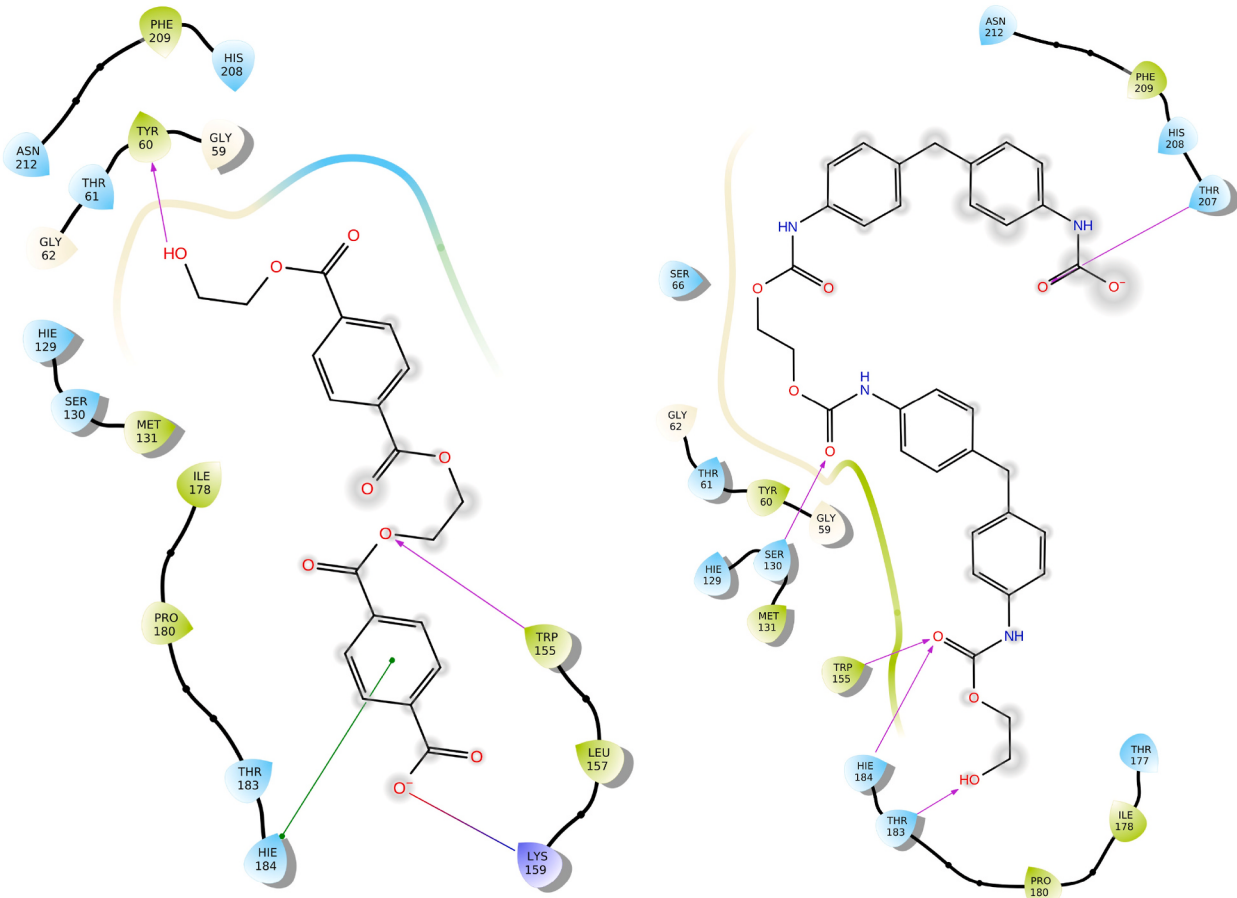


Fig. 4. The 2D interaction of (a) 4CG1_WT_PET and (b) 4CG1_WT_PU.

evident at 25 ns, 60 ns, and 75 ns. The highest deviation of 0.27 nm for 4CG1_N28M occurred around 73 ns. Complexes 4CG1_N28M_PET and 4CG1_N28M_PU remained intact, despite the deviations observed at 40 ns and 85 ns, respectively. These observations are depicted in Fig. 7 (a).

RMSF values of all the complexes were ≤ 0.25 nm, conferring insignificant changes overall. However, there were notable elevations in RMSF observed for N-terminal residues 1, 2, 3, 4, and C-terminal residues 260 to 263, reaching approximately 0.76 nm for complexes such as 4CG1_S136D_PU and other variants like 4CG1_S136Q_PU and 4CG1_N28M_PU. The 4CG1_S136Q variant showed relative fluctuation below 0.20 nm, with the 248th amino acid residue displaying the highest fluctuation around 0.1 nm. Similarly, complexes 4CG1_S136Q_PET and 4CG1_S136Q_PU showed insignificant deviation. In parallel, the N28M variant exhibited similar RMSF variations. Notably, RMSF values for all discussed structures converged to approximately 0.30 nm around the 131th amino acid position. This highlighted amino acid position (Figure S1 (a)) contains Serine, which serves as the catalytic site of cutinase [13].

The Radius of Gyration (R_g) serves as a critical metric for assessing the size and compactness of proteins, reflecting their molecular distribution (Fig. 7 (b)). While examining wild-type structures over a fixed time interval, consistent structural compactness was evident. Similarly, the mutated apoenzyme structure displayed stability, with a minor peak observed at 70 ns. However, 4CG1_WT_PET showed constant atomic distribution for the remaining duration. Conversely, 4CG1_WT_PU displayed slight fluctuation between 75 and 90 ns. The 4CG1_S136D_PET variant demonstrated increased gyration between 60 and 70 ns. The most compact structure among the S136D variants was 4CG1_S136D_PU. For the S136Q variant, 4CG1_S136Q_PU exhibited more consistent rotation compared to 4CG1_S136Q by 0.015 nm difference. Deviation peaks were noted for 4CG1_S136Q_PET around the 75–100 ns timeframe, with an R_g of 1.7 nm. The average R_g distribution for both the 4CG1_N28M_PU complex and 4CG1_N28M protein hovered around 1.675 nm, with nearly identical graphical patterns observed for these enzymes. Deviation in R_g values for the 4CG1_N28M_PET structure was observed around 40–80 ns, resembling the distribution pattern of 4CG1_S136Q_PET. Solvent-accessible surface area (SASA) signifies the portion of the protein accessible to solvent molecules [64]. Across all cases, a notable increase in SASA was observed, with maximum deviation noted for both ligands docked to wild type cutinase and mutated variants. Considering the WT cutinase complexes, the 4CG1_WT_PU exhibited the highest average SASA, while 4CG1_WT_PET displayed the lowest. Comparatively, the S136Q mutated proteins generally displayed lower SASA compared to their WT counterparts, with 4CG1_S136Q_PU registering the lowest average SASA among all the twelve cases discussed at 107 nm^2 . The most fluctuated SASA visualization was observed with the 4CG1_N28M_PU complex, followed

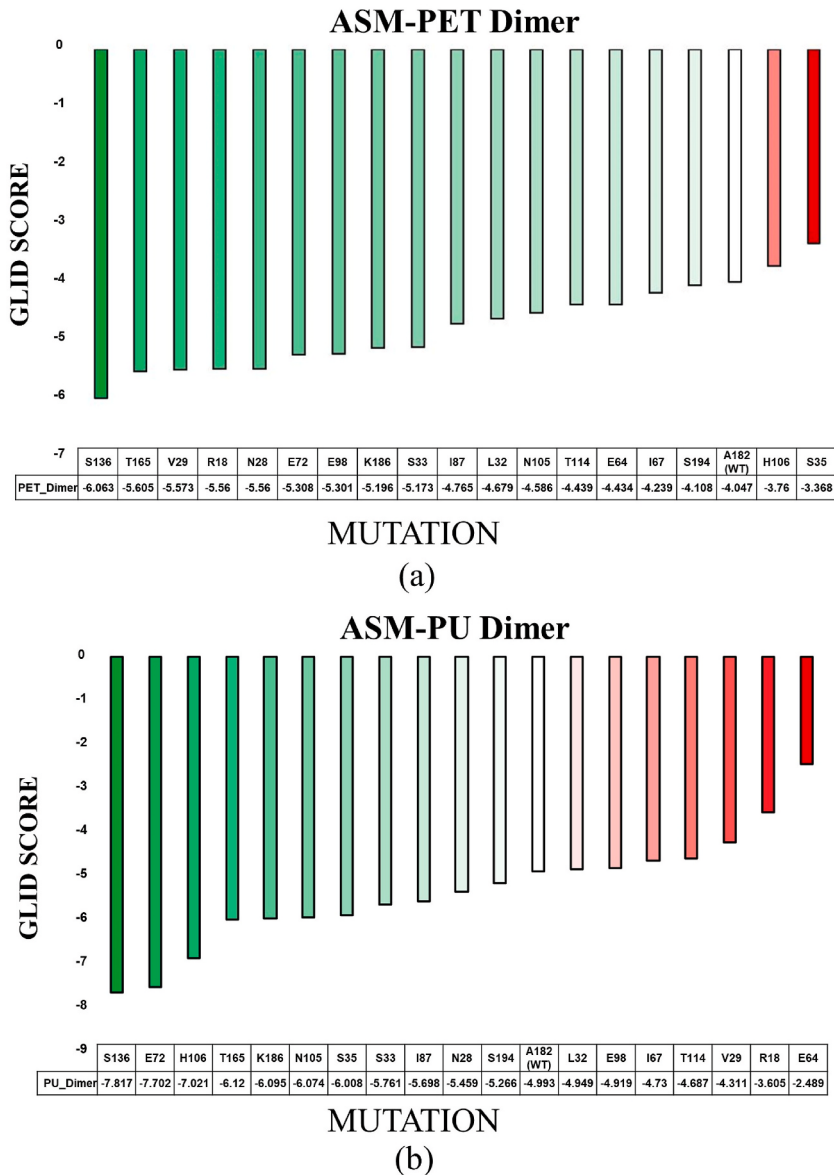
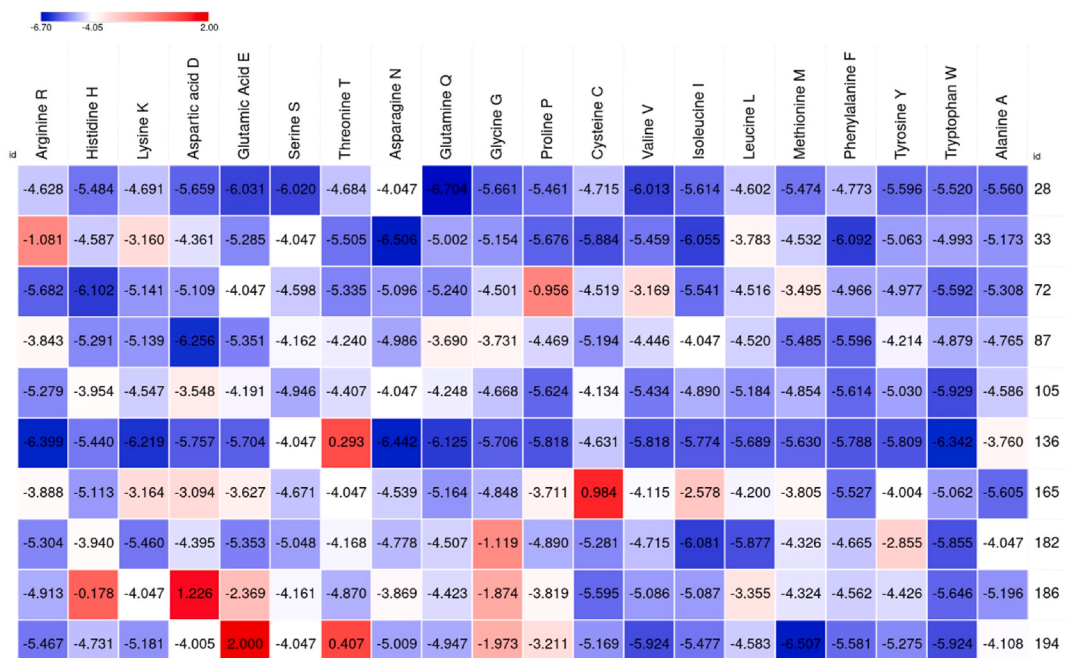


Fig. 5. The Alanine Scanning Mutagenesis (ASM) Schrödinger glide docking score values for (a) WT_protein_PET complex and (b) WT_protein_PU complex higher docking scores green and lower docking scores red.

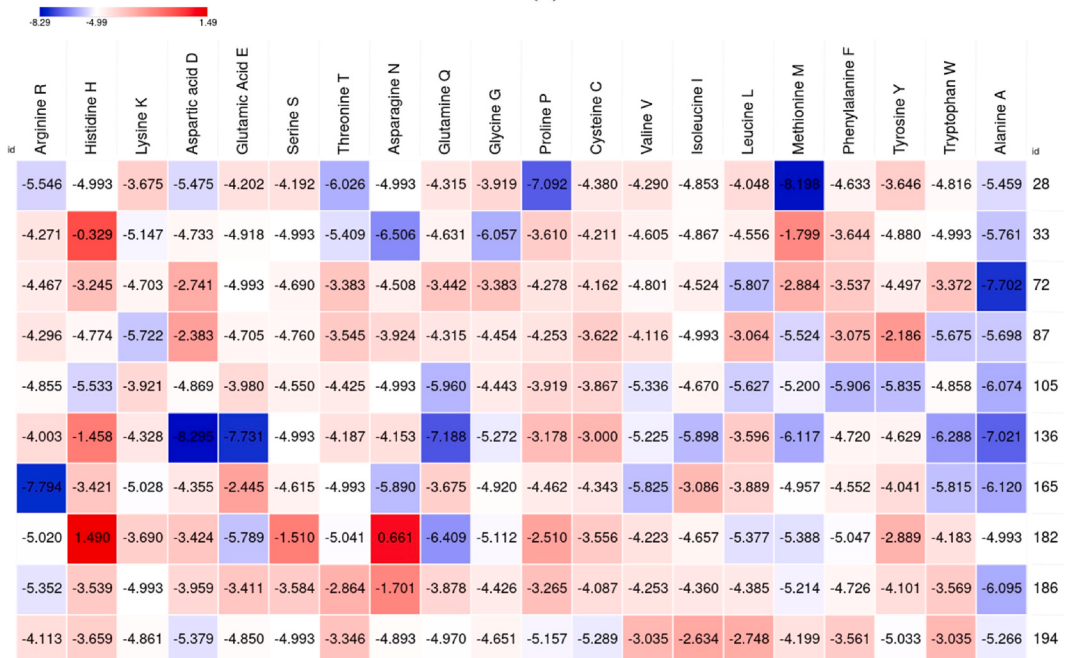
by 4CG1_N28M_PET, which exhibited similar patterns despite the apoenzyme of the variant displaying lower SASA, approximately around 108 nm². These observations are depicted graphically in Fig. 7 (c).

The strength of the complex interactions was discussed using the GROMACS energies along with number of hydrogen bonds present within the enzyme and its complexes [65]. The hydrogen bond numbers are depicted in Fig. 7(d). On average, the 4CG1_WT_PET complex exhibited approximately six hydrogen bonds within the 35 ns timeframe. 4CG1_WT_PU had one to three hydrogen bonds throughout the time 30–70 ns, although three to five hydrogen bonds were observed. Hydrogen bonds of two to three in number were maintained by the 4CG1_S136D_PET, 4CG1_S136D_PU and 4CG1_N28M_PU complexes throughout the simulation. The highlighted 4CG1_N28M_PET enzyme ligand complex was found to have a minimum of three hydrogen bonds with the highest number of five hydrogen bonds around 70 ns. The apoenzyme structures of S136Q and N28M i.e., 4CG1_S136Q and 4CG1_N28M were found to have at least one hydrogen bond. All the hydrogen bonds were revealed to have a bond length ≤0.35 nm according to the hydrogen bond distribution plot (Figure S1 (a)).

Consequently, the energy for the 4CG1_WT_PET complex was similar (-5.52×10^5 kJ/mol) to the energies of the other complexes. The GROMACS energies for the six structures of second and third best cases (4CG1_S136Q_PU, 4CG1_S136Q_PET, 4CG1_S136Q, 4CG1_N28M_PU, 4CG1_N28M_PET and 4CG1_N28M) were in the range of -5.5×10^5 kJ/mol. In general, the PU complex had minor



(a)



(b)

Fig. 6. SSM Schrodinger glide docking score: Heat map is drawn using MORPHEUS tool, (a) Mutated protein_PET complex, (b) Mutated protein_PU complex where the blue high docking scores and red low docking scores.

fluctuations compared to the PET variant. (Fig. 7 (e)).

Principal Component Analysis (PCA) offers a robust method for analysing conformational changes in proteins and their complexes. By tracking the motion of proteins and their ligand-bound forms in solution, PCA enables the differentiation between local fluctuations and collective movements that occur simultaneously [66]. 4CG1_WT complexes (both PET and PU) exhibited greater movement compared to the WT cutinase. 4CG1_WT_PET demonstrated values of approximately 7.5 nm and 3.5 nm in eigenvectors 1 and 2, respectively. Eigenvectors are the primary directions of motion or variations in the enzyme structure during molecular dynamics

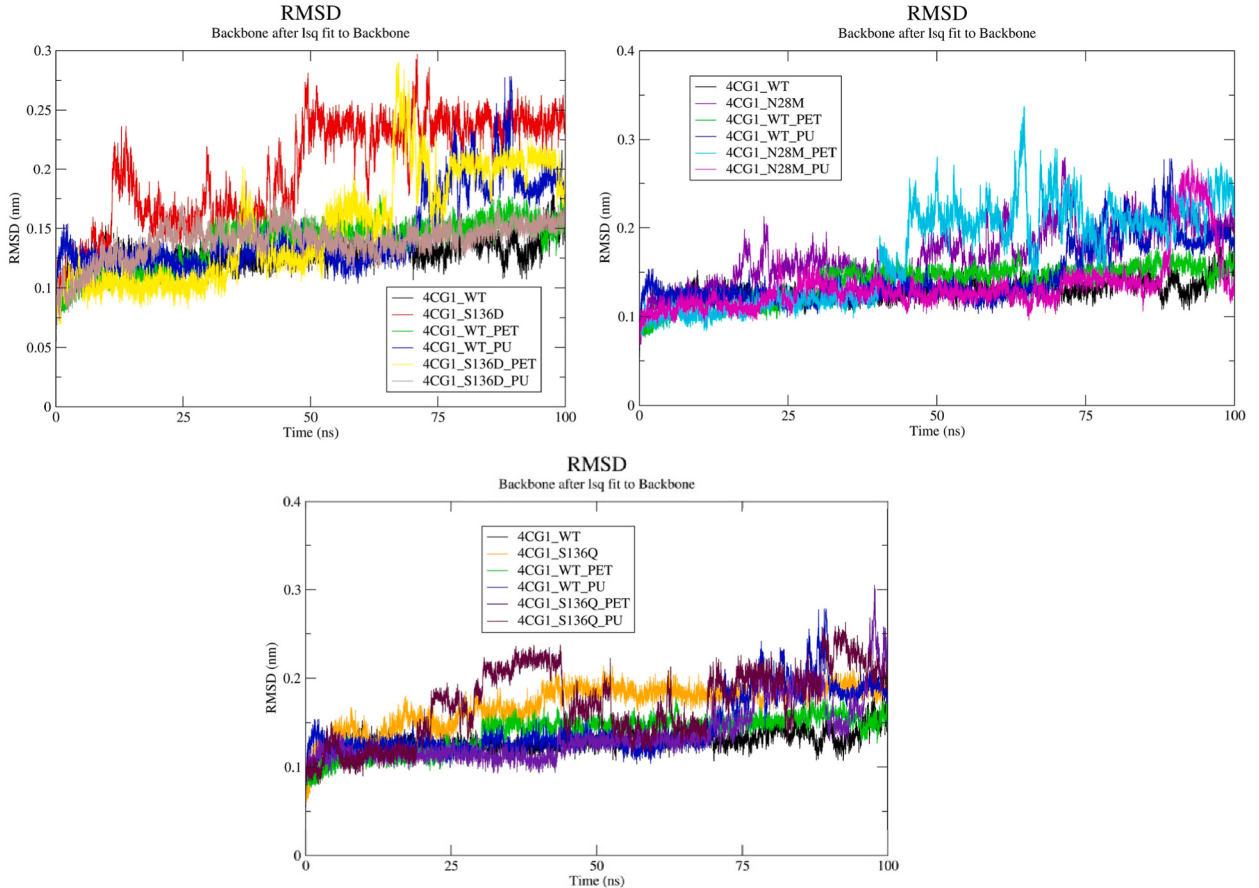


Fig. 7a. Root Mean Square Deviation (RMSD). Top left – comparison of WT protein, S136D variant protein and its complexes. Top right – comparison of WT protein with N28M variant protein and its complexes. Bottom – comparison of WT protein with S136Q variant protein and its complexes. 4CG1_WT (Black), 4CG1_WT_PET (Green), 4CG1_WT_PU (Dark blue), 4CG1_S136D (Red), 4CG1_S136D_PET (Yellow), 4CG1_S136D_PU (Brown), 4CG1_N28M (Violet), 4CG1_N28M_PET (Cyan), 4CG1_N28M_PU (Magenta), 4CG1_S136Q (Orange), 4CG1_S136Q_PET (Indigo) and 4CG1_S136Q_PU (Maroon). Same comparison and colour code are followed in all the results.

simulations. These orientations represent the enzyme-ligand complexes' most important conformational alterations. The first few principal components (PCs) record the enzyme's major movements, such as binding pocket flexibility or large-scale conformational alterations, which are frequently related to the enzyme's functional state. By evaluating the eigenvectors, we can identify sections of the protein that undergo the most significant structural changes, which can be linked to increased or decreased binding affinity. Remarkably, the 4CG1_WT_PU complex displayed a movement reaching 12.5 nm in eigenvector 2. Conversely, the movement of the 4CG1_S136D_PU complex appeared more constrained compared to 4CG1_S136D_PET, which achieved approximately -12.5 nm in eigenvector 2 and 8 nm in eigenvector 1. A similar trend was observed in 4CG1_N28M complexes. Both 4CG1_S136Q_PET and 4CG1_S136Q_PU attained -5 nm in eigenvector 2. However, 4CG1_S136Q_PU exhibited a higher value of approximately 7.5 nm in eigenvector 1 compared to 4CG1_S136Q_PET. These findings confirm that ligand interaction enhances the movement of cutinase, as depicted in Fig. 8 for all twelve complexes.

The Free Energy Landscapes (FEL) plot serves to analyse the binding affinities of protein-ligand interactions, pinpointing low-energy basins known as energy minima. In this visualization, the violet-coloured lower peaks denote energy minima, indicating energetically favourable conformations of the protein-ligand complexes. Conversely, regions shaded in red to yellow represent energetically unfavourable conformations [67].

Although four peaks were obtained for each protein-ligand complex of both WT cutinase and variants, only one peak image is provided in the FEL (Figures S2(a) and S2(b)). One hydrogen bond was formed at both the peaks 65,090 ps and 65,200 ps by Q92 and S130, respectively. In 4CG1_S136D_PET, two connected plateaus with stable energy levels ranging from -3.006 to -3.820 kcal/mol were observed (Figure S2(c)). Among the four peaks identified, the 2D structure at 58,640 ps revealed a hydrogen bond between residue Q92 and the ligand's OH group. In contrast, 4CG1_S136D_PU displayed three connected energy minima within the energy range of -2.580 to -3.200 kcal/mol (Figure S2(d)). Analysis of the 2D structures showed three hydrogen bonds at 15,790 ps and 15,970 ps, involving residues T207, N215, Y60, and S130. Peaks at 16,200 ps and 16,700 ps exhibited one and two hydrogen bonds, respectively, with N212 forming a hydrogen bond at 16,700 ps. Additionally, Y60 and N212 formed hydrogen bonds at 16,700 ps. The

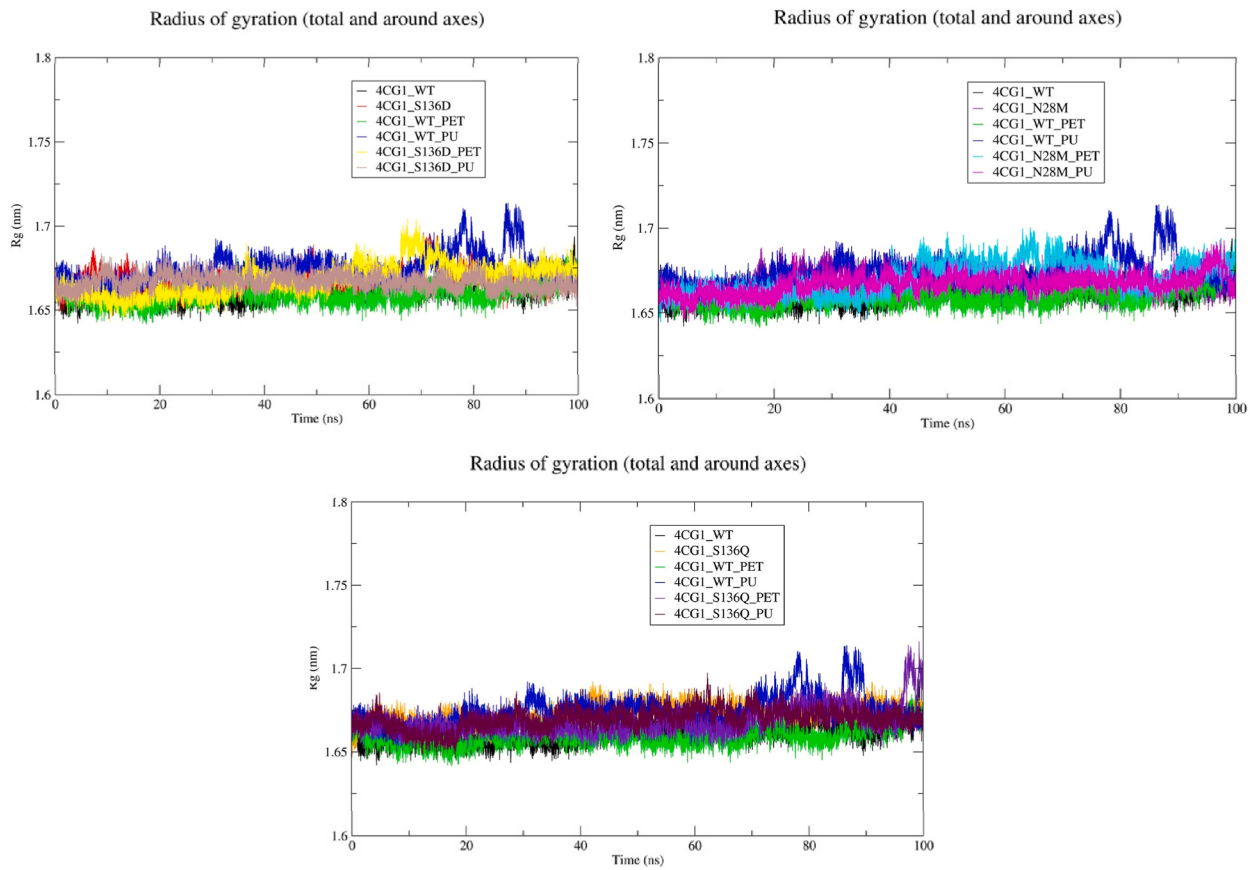


Fig. 7b. Radius of gyration.

second-best case (4CG1_N28M_PET and 4CG1_N28M_PU) has two distinct sharp peaks and two clustered peaks, respectively. Stable energy ranges for these complexes were observed between -2.328 and -2.960 kcal/mol for 4CG1_N28M_PET and -2.026 to -2.600 kcal/mol for 4CG1_N28M_PU (Figures S2(e) and S2(f)). In 4CG1_N28M_PET, hydrogen bonds between residues H156 and R138 were depicted in the 2D structures at peaks 66,070 ps and 66,080 ps, while no interactions were observed at 66,090 ps and 66,110 ps. The 2D structures of all the peaks of 4CG1_N28M_PU depicted a single hydrogen bond interaction between the ligand and the residue T61. In 4CG1_S136Q_PET, four distinct clustered plateaus were observed, while in 4CG1_S136Q_PU, a single broad shoulder was noticed. These are considered as energy minima. The residue Q92 was a common residue that participated in the hydrogen bond formation in the complex 4CG1_S136Q_PET's 2D structure (Figure S2 (g)). However, N212 also formed a hydrogen bond at the peak 36,150 ps. Additionally, W155 and Y60 formed a hydrogen bond at the peak of 48,760 ps. The 2D structures of the peaks 65,020 ps and 65,030 ps of the complex 4CG1_S136Q_PU did not show any interaction (Figure S2 (h)).

In molecular dynamics (MD) simulations, determining a system's solvation-free energy often involves employing the Poisson-Boltzmann (PB) and Generalized Born (GB) solvation models. To enhance the accuracy of this estimation, MM-PBSA (Molecular Mechanics/Poisson-Boltzmann Surface Area) and MM-GBSA (Molecular Mechanics/Generalized Born Surface Area) approaches are commonly employed [68]. The decomposition analysis of per-residue contributions was conducted using the standard Poisson-Boltzmann (PB) energy model, including the total decomposition contribution (TDC) and the side-chain decomposition contribution (SDC) G. et al. [69]. Certain residues are consistently involved across different mutations and ligand-bound states, according to the TDC analysis in various 4CG1 complexes. The residues Y60, H129, W155, H184, H208, F209, and N212 were shown to be the significant contributors to the highest interaction energies in all complexes examined, indicating their critical function in preserving stable ligand binding. They were consistently among the top donors to interaction energies for the 4CG1_WT_PET and 4CG1_WT_PU complexes (Figures S3(a) and S3(b)). Similarly, the identical core residues and D176 in the PU form demonstrated substantial interaction energies in the 4CG1_S136D_PET and 4CG1_S136D_PU complexes (Figures S4(a) and S4(b)). Similar patterns were seen in the 4CG1_N28M_PET and 4CG1_N28M_PU complexes (Figures S5 (a) and S5(b)), where Y60, H129, W155, H184, H208, F209, and N212 were prevalent. However, D176 was noteworthy in the PU state again. With the addition of G205, A206, and A210 in the PU complex, the core residues for the 4CG1_S136Q_PET and 4CG1_S136Q_PU complexes (Figures S6 (a) and S6 (b)) continued to have significant interaction energy contributions, further demonstrating the impact of particular mutations on the binding interface. Although other residues differ among the various complexes, the core residues Y60, H129, W155, H184, H208, F209, and N212 are consistently in charge of the strongest interactions, indicating that they play a crucial role in maintaining the protein-ligand

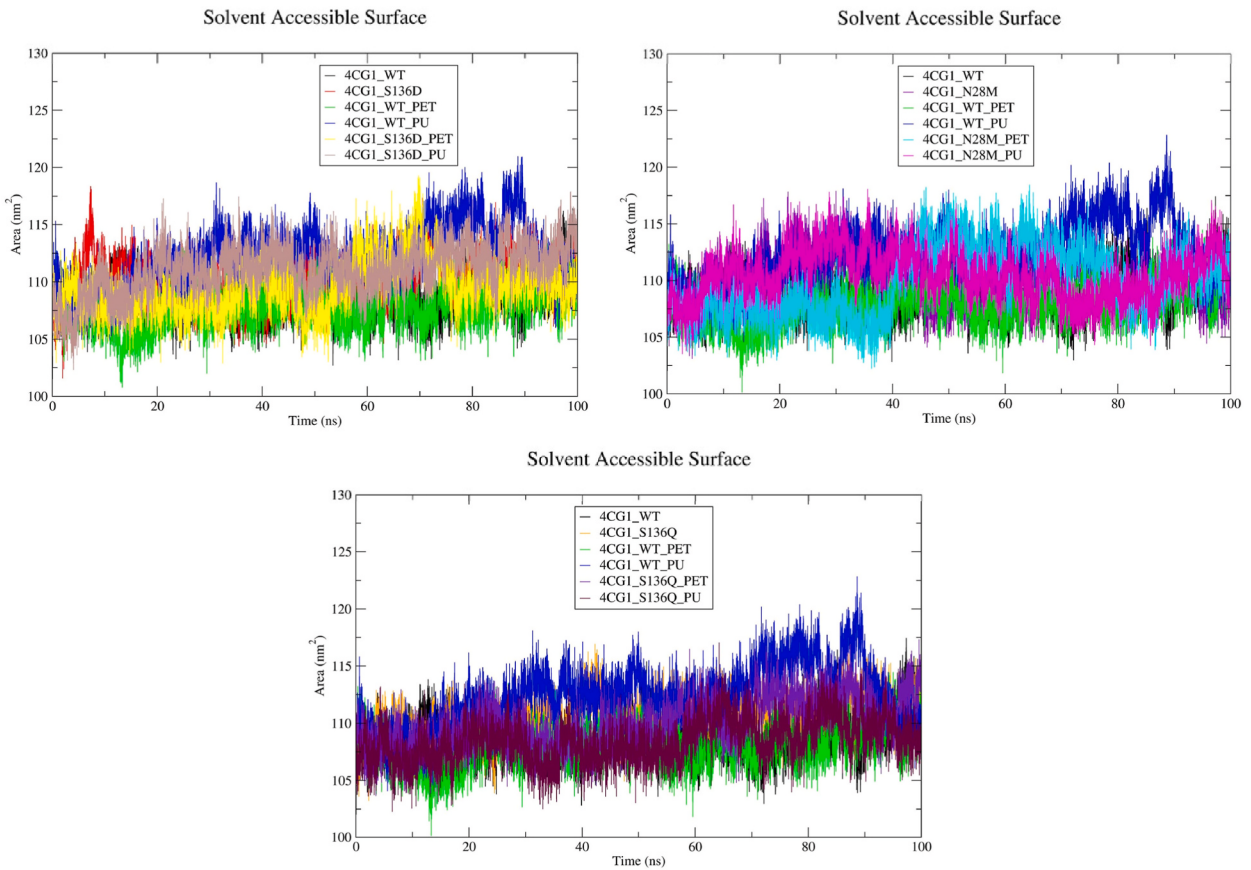


Fig. 7c. Solvent accessible surface area (SASA).

interactions in all complexes under study.

Furthermore, we incorporated MMGBSA which is the combination of the probability of free ligand-protein interactions and the influence of the solution. Coulomb energy, covalent binding energy, van der Waals energy, and lipophilic energy all contribute to the solution's composition [69,70]. As per the findings presented in Table S1, it is evident that the 4CG1_S136D_PU complex demonstrates superior ligand binding efficiency in the MMGBSA analysis compared to the other complexes under investigation.

3.8. PRODIGY

PRODIGY prediction revealed the binding affinity of the selected WT protein complexes and the corresponding mutated variant protein complexes with their respective ligands, namely, PET and PU. The results showed an improvement in the binding affinity of the mutated variant protein-ligand complexes compared to WT-ligand complexes (Table S2).

4. Discussion

In this study, different plastic degrading microbial enzymes capable of degrading plastics, such as PE, PET, PVC, and PU, were enlisted. Among all these enzymes, cutinase (PDB ID: 4CG1) from *T. fusca* was selected for detailed simulation studies due to its ability to bind with both PET and PU polymers. It has been shown to exhibit diverse hydrolytic activity, strong surfactant tolerance, remarkable stability in organic solvents, and excellent thermostability, indicating its potential utility in plastic degradation [71]. The natural ability of the enzyme to degrade PET and PU has been reported by Roth et al. (2014b) and Schmidt et al. (2017b), making it a promising bifunctional enzyme.

PET degradation typically involves cleavage into bis-(2-hydroxyethyl) terephthalate (BHET) and terephthalic acid (TPA), with BHET further breaking down into TPA and Ethylene glycol (EG) [72]. Previous research suggests that TPA and EG can either be assimilated by microorganisms for metabolic utilization or converted into high-value chemicals [73]. Notably, our molecular docking studies revealed interactions between specific residues, such as T61 and W155, with oxygen atoms (Fig. 4 (a)), potentially indicating nucleophilic attacks and subsequent catalytic reactions [74]. Likewise, in WT-PU complexes (Fig. 4 (b)), hydrogen bonds involving N212 and hydrophobic interactions with other residues near the carbonyl oxygen may facilitate urethane bond hydrolysis [34]. The

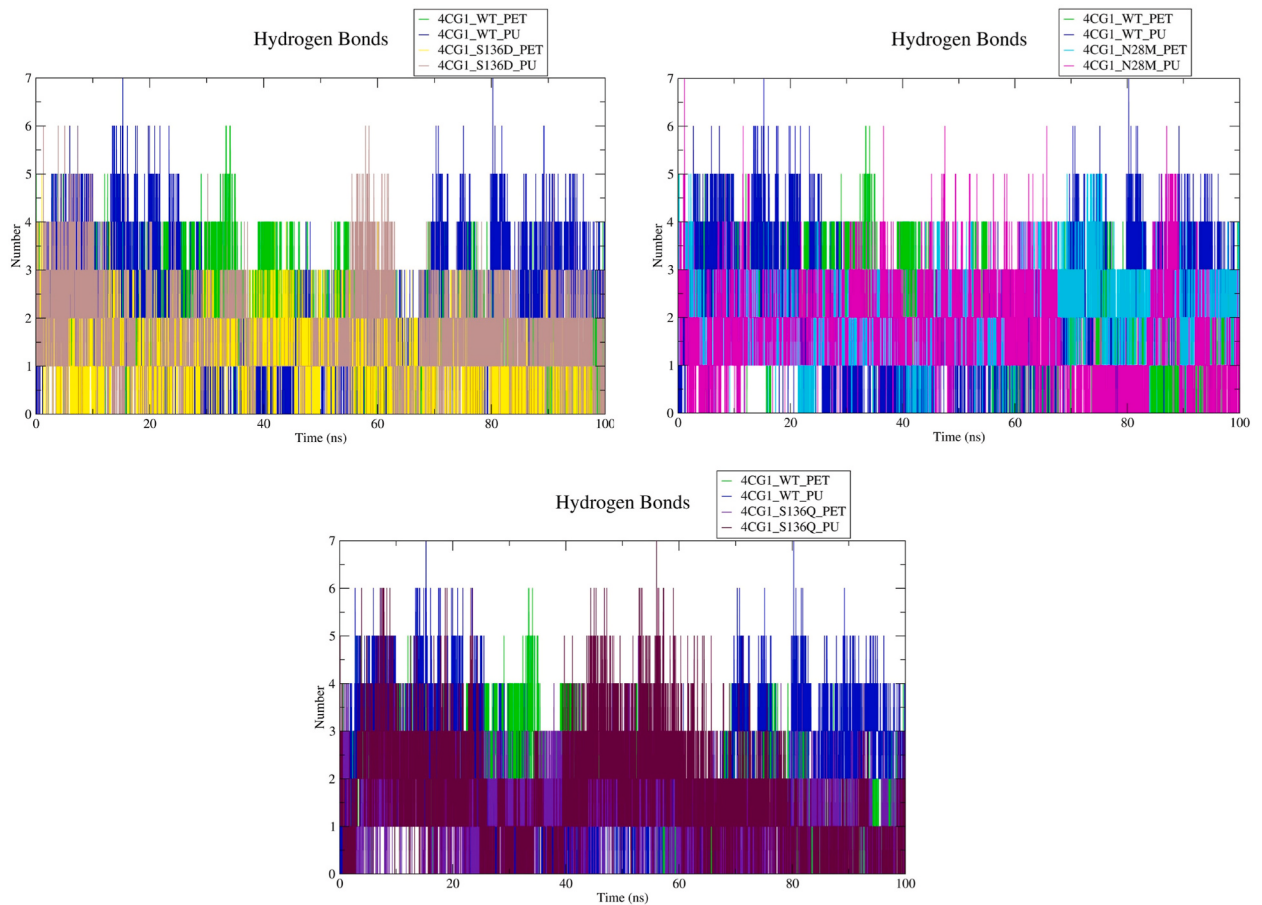


Fig. 7d. Hydrogen bonds.

formation of hydrogen bonds between the active site and ligand molecule may indicate the occurrence of the cleaving activity of the enzyme. Despite these interactions, the initial docking scores for WT enzyme-ligand complexes were sub-optimal, prompting us to explore mutations in unconserved regions of the enzyme to enhance binding affinity. These unconserved regions play pivotal roles in functional divergence during enzyme evolution [75]. Consequently, our study focused on identifying mutations that either augment or compromise cutinase activity towards PET and PU ligands. Through comprehensive screening tests, including primary (ASM) and secondary (SSM) screenings, we identified the most promising variants—S136D, N28M, and S136Q—exhibiting improved binding affinities towards both PET and PU ligands (Figs. 5 and 6). Additionally, structural analyses revealed a transition from alpha helix to random coil in all variants, with the S136D variant displaying increased structural flexibility, potentially contributing to enhanced ligand binding [76]. This explains the hollow appearance of the variant enzymes that could have aided in the higher binding affinity of the ligands. However, further studies are required to validate this hypothesis.

The Rg values exhibited minimal variance among the WT cutinase, variants, and their respective ligands, indicating the structural compactness of the variants and their complexes despite the presence of additional loops and a hollow structure compared to the WT enzyme.

The binding pockets of the variants, as observed using CASTp were as follows: S136D: Area = 56.827 Å² and Volume = 16.027 Å³, N28M: Area = 56.827 Å² and Volume = 15.954 Å³, and S136Q: Area = 57.482 Å² and 16.883 Å³ and for the WT Area = 72.687 Å² and Volume = 20.917 Å³. In spite of the reduced binding pocket size, the TDC graphs (Figure S3) show the contribution of the active site and binding site throughout the stipulated time of simulation.

The binding sites and the active sites of the enzyme are Y60, M131, W155 and S130, D176, H208, respectively. The WT_PET complex had energy contribution from the residues Y60, M131, W155, S130, and H208, while the WT_PU complex had energy contribution from the residues Y60, M131, W155, and H208. The variants PET complexes established similar energy contributions with the same residues at the active and binding sites (except S136D_PET which did not have M131), In contrast, the variant PU complexes established energy contribution from all residues Y60, M131, W155, S130, D176, and H208 (except S136Q which did not have D176). This explains the higher binding affinity of PU ligand to the variants. Moreover, we observed that the binding affinity of both the ligands improved despite the structural changes in the variants.

Further insights into structural compactness were unveiled through Principal Component Analysis (PCA) of WT, variants, and their

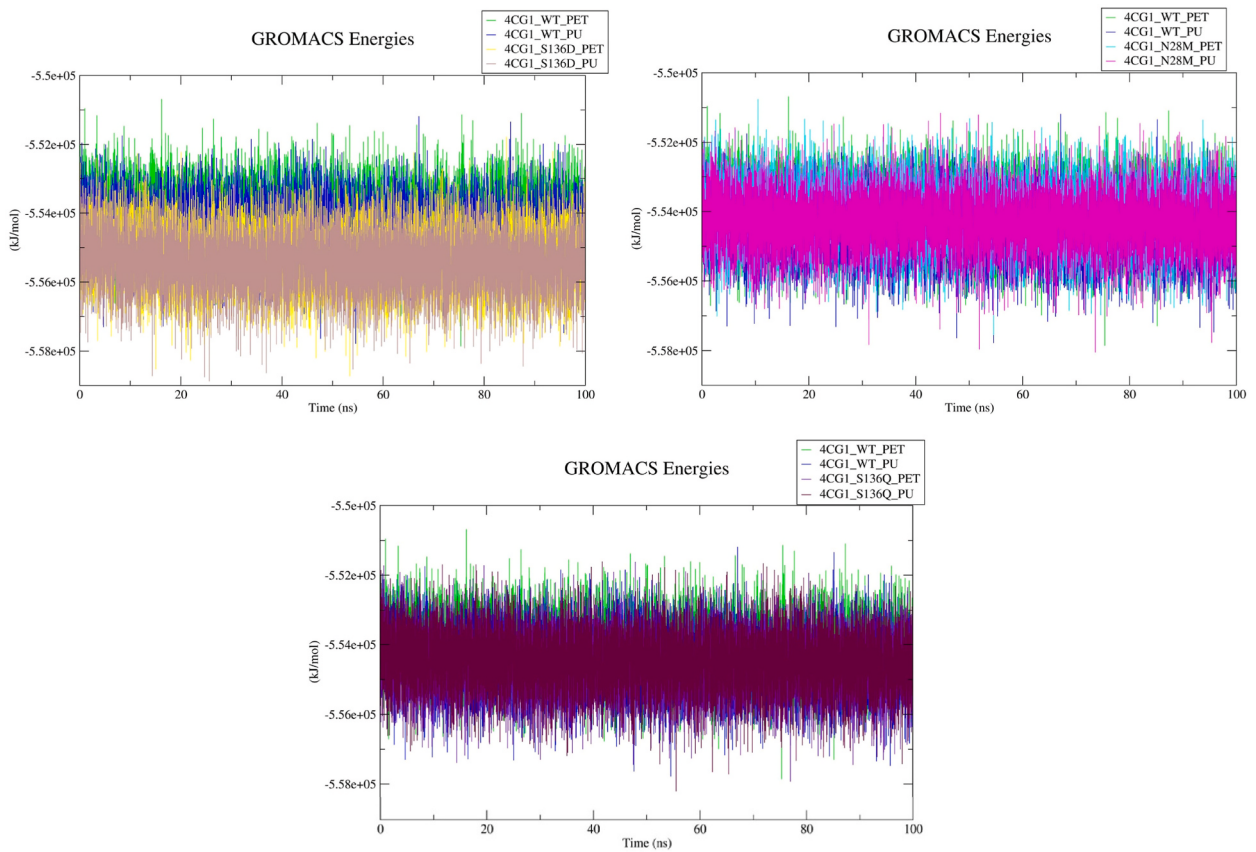


Fig. 7e. Interaction energies.

ligand complexes. Notably, the range of eigenvectors 1 and 2 differed for each variant and their ligand complexes, surpassing that of the WT cutinase and its variants. This suggests that the mutated complexes exhibited a lot of motions inside the simulation environment.

In general, hydrogen bonds between the enzyme and ligand enhance ligand binding [77]. However, the hydrogen bond distribution contradicts with WT cutinase and its variants between docking studies and MDS. Although the number of hydrogen bonds was lower in mutated complexes, their consistent retention throughout the simulation likely contributed to their higher binding affinity. More fluctuations in hydrogen bond distributions were also seen with WT compared to the mutated complexes. Similarly, the mutated complexes could have had more motion in the simulation box in order to retain the hydrogen bonds.

The WT cutinase had lower RMSD values than the variants. Nevertheless, the maximum RMSD (0.3 nm) was obtained during the 100 ns simulation, which may reveal the stability of the cutinase (Fig. 7 (a)). The RMSF also indicates cutinase stability at residue level (Figure S1 (b)).

GROMACS energies (Fig. 7 (e)) revealed that the WT and the variant complexes were in a similar energy range, but the energy fluctuations of variant complexes were observed to be less. MM-PBSA results give the free energy contribution of each residue to the ligand binding [78]. The residue contribution of both WT and variant complexes was similar. But PU ligand had higher energy (-600 kcal/mol) than PET ligand (-260 kcal/mol). This correlates with the higher docking scores obtained for PU ligand complexes than PET ligand complexes.

Our results affirm the increased stability of variants with PET and PU ligands. The binding affinity scores obtained from PRODIGY (Table S2) show that the binding energy PET and PU were increased significantly in the N28M mutated variant compared to the other two variants. This correlates with the docking scores obtained, where the N28M variant improved the binding affinity of both PET and PU. A comparison of Schrodinger glide score with Auto Dock Vina Wizard Score was obtained for the chosen complexes, and the results are presented in Table S3.

Cumulatively, the variants and their complexes remained persistent in terms of structural compactness, stability, interaction and binding energy. Particularly, the variant of cutinase (N28M) showed significant improvement in terms of binding affinity and stability with both PET and PU ligands. We acknowledge that, while our docking and molecular dynamics simulations provide enzyme binding affinity and stability, they do not capture the full enzyme dynamics required for catalysis. This limitation may result in discrepancies between *in silico* predictions and wet lab results. Our findings offer valuable guidance for developing effective enzymes for plastic degradation, but they do not account for environmental factors like pH, temperature and substrate concentration. To address this, we

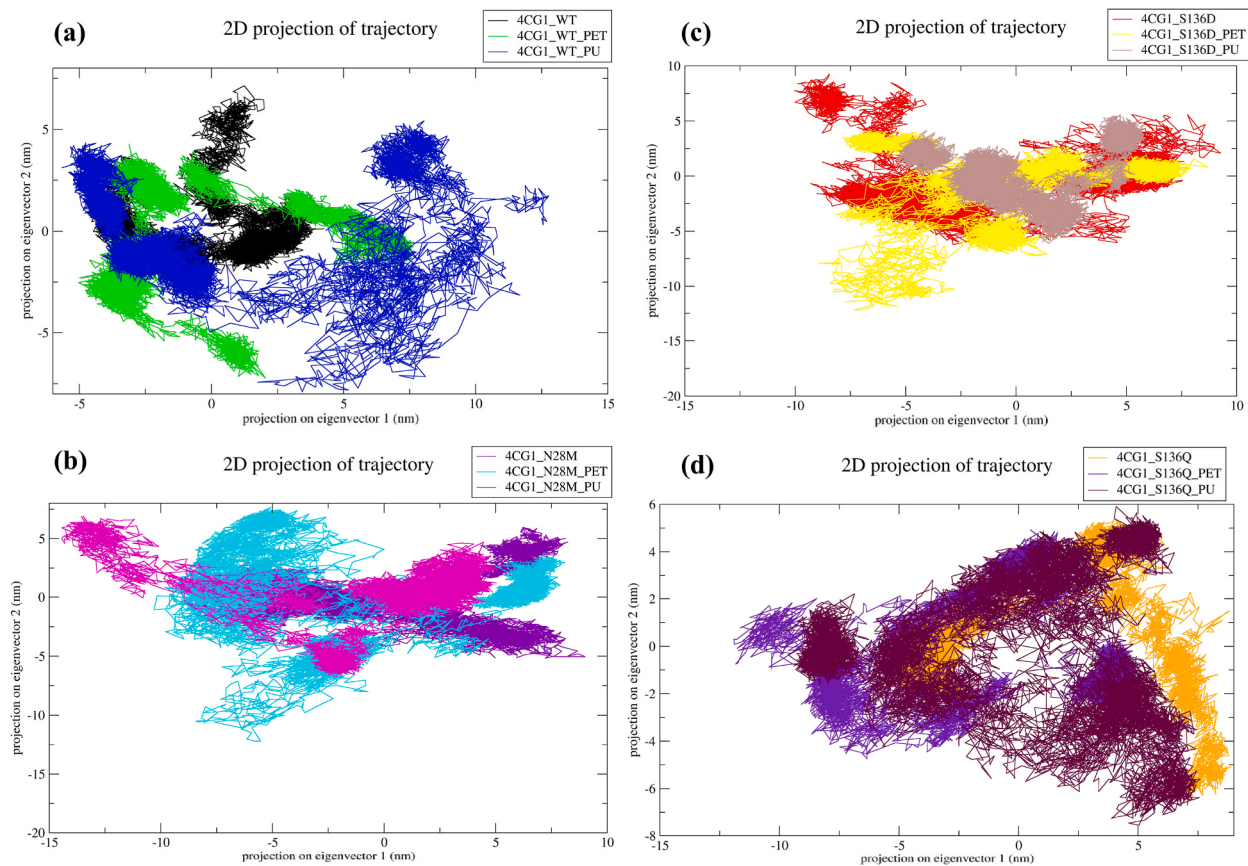


Fig. 8. Principal Component Analysis ([PCA]) of protein ligand complexes. (a) 4CG1_WT, (b) 4CG1_S136D, (c) 4CG1_N28M, and (d) 4CG1_S136Q.

recommend using advanced techniques such as accelerated molecular dynamics (aMD) or quantum mechanics/molecular mechanics (QM/MM) in future research. These predictions serve as an initial screening of promising enzyme variants and further *in vitro* and *in vivo* testing is needed to confirm the results and optimize enzyme function in real-world conditions.

5. Conclusion

The rampant surge in plastic consumption in recent years has led to an alarming increase in plastic pollution. The lack of effective degradation techniques has perpetuated the problem. Microbial enzymatic degradation emerges as a promising solution to combat pollution. Due to the indiscriminate dumping of various kinds of plastics in landfills, the segregation of plastics is complicated and challenging. Therefore, a MPD enzyme becomes a necessity. In this *in-silico* work, such an enzyme, *T. Fusca* cutinase, was identified, and its binding affinities towards its ligands PET and PU were improved along with its stability by mutations. Our docking and molecular dynamics simulations revealed important information on the structural stability, binding interactions and possible hydrolytic activity of these enzyme variants, indicating their potential in plastic degradation applications. While the simulations indicate that the N28M mutant variant could be more efficient for plastic degradation, we acknowledge that these results are preliminary. This study presents a computational approach to enhance enzyme activity for plastic degradation, identifying key modifications that may improve both binding and catalytic efficiency. Our findings demonstrate the potential of using molecular docking and binding free energy analyses to predict enzyme-plastic interactions, providing a valuable theoretical foundation. Although experimental validation is needed to confirm these predictions, this work serves as a step toward sustainable enzymatic solutions for plastic waste management. Thus, these mutated variants have the potential to improve the degrading properties of the enzyme, which can be assured in future *in vitro* studies, paving the way for practical application in environmental biodegradation.

CRediT authorship contribution statement

Deves Sabari V L: Writing – original draft, Visualization, Methodology, Investigation, Formal analysis, Conceptualization. **Gokulnath Rajmohan:** Methodology, Investigation. **Roshine S B:** Methodology, Investigation. **Srivaishnavi S:** Methodology, Investigation. **Kishore Nagasubramanian:** Visualization, Methodology, Investigation, Data curation. **Senthil Kumar G:** Writing –

original draft, Visualization, Software, Project administration, Data curation, Conceptualization. **Ponnusami Venkatachalam:** Writing – review & editing, Supervision, Methodology, Formal analysis, Conceptualization.

Declaration of competing interest

The authors declare the following financial interests/personal relationships which may be considered as potential competing interests: Ponnusami Venkatachalam reports financial support was provided by India Ministry of Science & Technology Department of Biotechnology. Prof. Ponnusami Venkatachalam, the corresponding author is a member of the Editorial Advisory Board, Heliyon Chemical Engineering section, Heliyon. If there are other authors, they declare that they have no known competing financial interests or personal relationships that could have appeared to influence the work reported in this paper.

Acknowledgement

The authors acknowledge the Department of Biotechnology (Grant No. BT/PR40144/BTIS/137/46/2022), The Government of India, and SASTRA Deemed University for providing the Schrodinger software and computational resources.

Appendix A Supplementary data

Supplementary data to this article can be found online at <https://doi.org/10.1016/j.heliyon.2025.e41640>.

References

- [1] S.S. Ali, E.A. Abdelkarim, T. Elsamahy, R. Al-Tohamy, F. Li, M. Kornaros, A. Zuorro, D. Zhu, J. Sun, Bioplastic production in terms of life cycle assessment: a state-of-the-art review, *Environmental Science and Ecotechnology* 15 (2023) 100254, <https://doi.org/10.1016/j.ese.2023.100254>.
- [2] P.F. Britt, G.W. Coates, K.I. Winey, J. Byers, E. Chen, B. Coughlin, C. Ellison, J. Garcia, A. Goldman, J. Guzman, J. Hartwig, B. Helms, G. Huber, C. Jenks, J. Martin, M. McCann, S. Miller, H. O'Neill, A. Sadow, R. Waymouth, Report of the basic energy Sciences Roundtable on chemical Upcycling of polymers, <https://doi.org/10.2172/1616517>, 2019.
- [3] Y.-Y. Lai, Y.-M. Lee, Management strategy of plastic wastes in Taiwan, *Sustainable Environment Research* 32 (1) (2022) 11, <https://doi.org/10.1186/s42834-022-00123-0>.
- [4] J. Kaushal, M. Khatri, S.K. Arya, Recent insight into enzymatic degradation of plastics prevalent in the environment: a mini - review, *Cleaner Engineering and Technology* 2 (2021) 100083, <https://doi.org/10.1016/j.clet.2021.100083>.
- [5] H. Wang, F. Guan, Y. Zhu, Y. Pan, Q. Liu, Q. Liu, W. He, D. Gong, J. Tian, D. Han, Biofilm formation promoted biodegradation of polyethylene in *Gordonia polyisoprenivorans* B251 isolated from bacterial enrichment acclimated by hexadecane for two years, *Chemosphere* 344 (2023) 140383, <https://doi.org/10.1016/j.chemosphere.2023.140383>.
- [6] C.E. Enyoh, P.E. Ovuoraye, M.H. Rabin, W. Qingyue, M.A. Tahir, Thermal degradation evaluation of polyethylene terephthalate microplastics: insights from kinetics and machine learning algorithms using non-isothermal TGA data, *J. Environ. Chem. Eng.* 12 (2) (2024) 111909, <https://doi.org/10.1016/j.jece.2024.111909>.
- [7] J. Song, J. Wang, J. Sima, Y. Zhu, X. Du, P.T. Williams, Q. Huang, Dechlorination of waste polyvinyl chloride (PVC) through non-thermal plasma, *Chemosphere* 338 (2023) 139535, <https://doi.org/10.1016/j.chemosphere.2023.139535>.
- [8] T. Ahmad, X. Liu, C. Guria, Preparation of polyvinyl chloride (PVC) membrane blended with acrylamide grafted bentonite for oily water treatment, *Chemosphere* 310 (2023) 136840, <https://doi.org/10.1016/j.chemosphere.2022.136840>.
- [9] J. Li, H. Zhu, D. Fang, X. Huang, C. Zhang, Y. Luo, Mechanochemistry recycling of polyurethane foam using urethane exchange reaction, *J. Environ. Chem. Eng.* 11 (3) (2023) 110269, <https://doi.org/10.1016/j.jece.2023.110269>.
- [10] A. Nakkabi, M. Sadiki, I. Koraichi, H. Barkai, E. Abed, Biodegradation of Poly(ester urethane)s by *Bacillus subtilis*, *Int. J. Environ. Res. 9* (1) (2015) 157–162.
- [11] J. Ji, J. Pei, F. Ding, C. Zeng, J. Zhou, W. Dong, Z. Cui, X. Yan, Isolation and characterization of polyester polyurethane-degrading bacterium *Bacillus* sp. YXP1, *Environ. Res.* 249 (2024) 118468, <https://doi.org/10.1016/j.envres.2024.118468>.
- [12] G. Gourmelon, *Global Plastic Production Rises, Recycling Lags* (2015).
- [13] G. Martínez-Narro, S. Hassan, A.N. Phan, Chemical recycling of plastic waste for sustainable polymer manufacturing – a critical review, *J. Environ. Chem. Eng.* 12 (2) (2024) 112323, <https://doi.org/10.1016/j.jece.2024.112323>.
- [14] E. Naderi Kalali, S. Lotfian, M. Entezar Shabestari, S. Khayatzadeh, C. Zhao, H. Yazdani Nezhad, A critical review of the current progress of plastic waste recycling technology in structural materials, *Curr. Opin. Green Sustainable Chem.* 40 (2023) 100763, <https://doi.org/10.1016/j.cogsc.2023.100763>.
- [15] D. Pan, F. Su, C. Liu, Z. Guo, Research progress for plastic waste management and manufacture of value-added products, *Advanced Composites and Hybrid Materials* 3 (4) (2020) 443–461, <https://doi.org/10.1007/s42114-020-00190-0>.
- [16] D. March, K. Metcalfe, J. Tintoré, B.J. Godley, Tracking the global reduction of marine traffic during the COVID-19 pandemic, *Nat. Commun.* 12 (1) (2021) 2415, <https://doi.org/10.1038/s41467-021-22423-6>.
- [17] V. Tournier, S. Duquesne, F. Guillamot, H. Cramail, D. Taton, A. Marty, I. André, Enzymes' Power for plastics degradation, *Chem. Rev.* 123 (9) (2023) 5612–5701, <https://doi.org/10.1021/acs.chemrev.2c00644>.
- [18] A. Amobonye, P. Bhagwat, S. Singh, S. Pillai, Plastic biodegradation: Frontline microbes and their enzymes, *Sci. Total Environ.* 759 (2021) 143536, <https://doi.org/10.1016/j.scitotenv.2020.143536>.
- [19] A.L. Pometto, B.T. Lee, K.E. Johnson, Production of an extracellular polyethylene-degrading enzyme(s) by *Streptomyces* species, *Appl. Environ. Microbiol.* 58 (2) (1992) 731–733, <https://doi.org/10.1128/aem.58.2.731-733.1992>.
- [20] A. Bollinger, S. Thies, E. Knieps-Grünhagen, C. Gertzen, S. Kobus, A. Höppner, M. Ferrer, H. Gohlke, S.H.J. Smits, K.-E. Jaeger, A novel polyester hydrolase from the marine bacterium *Pseudomonas aestuarii* – structural and functional insights, *Front. Microbiol.* 11 (2020), <https://doi.org/10.3389/fmicb.2020.00114>.
- [21] C. Liu, C. Shi, S. Zhu, R. Wei, C.-C. Yin, Structural and functional characterization of polyethylene terephthalate hydrolase from *Ideonella sakaiensis*, *Biochem. Biophys. Res. Commun.* 508 (1) (2019) 289–294, <https://doi.org/10.1016/j.bbrc.2018.11.148>.
- [22] A. Barclay, K.R. Acharya, Engineering plastic eating enzymes using structural Biology, *Biomolecules* 13 (9) (2023) 1407, <https://doi.org/10.3390/biom13091407>.
- [23] Y. Tang, W. Zhu, K. Chen, H. Jiang, New technologies in computer-aided drug design: toward target identification and new chemical entity discovery, *Drug Discov. Today Technol.* 3 (3) (2006) 307–313, <https://doi.org/10.1016/j.ddtec.2006.09.004>.

- [24] B. Shaker, S. Ahmad, J. Lee, C. Jung, D. Na, In silico methods and tools for drug discovery, *Comput. Biol. Med.* 137 (2021) 104851, <https://doi.org/10.1016/j.combiopharm.2021.104851>.
- [25] A. Amberg, In silico methods, in: *Drug Discovery and Evaluation: Safety and Pharmacokinetic Assays*, Springer Berlin Heidelberg, 2013, pp. 1273–1296, https://doi.org/10.1007/978-3-642-25240-2_55.
- [26] M. Moradi, R. Golmohammadi, A. Najafi, M. Moosazadeh Moghadam, M. Fasihi-Ramandi, R. Mirnejad, A contemporary review on the important role of in silico approaches for managing different aspects of COVID-19 crisis, *Inform. Med. Unlocked* 28 (2022) 100862, <https://doi.org/10.1016/j.imu.2022.100862>.
- [27] C.E. Enyoh, T.O. Maduka, C.E. Duru, S.C. Osigwe, C.B.C. Ikpa, Q. Wang, In silico binding affinity studies of microbial enzymatic degradation of plastics, *Journal of Hazardous Materials Advances* 6 (2022) 100076, <https://doi.org/10.1016/j.hazadv.2022.100076>.
- [28] B. Kasemo, *Biological surface science*, *Surf. Sci.* 500 (1–3) (2002) 656–677.
- [29] L. Vrman, A.L. Adams, “Identification of rapid changes at plasma-solid interfaces, *J. Biomed. Mater. Res.* 3 (1) (1969) 43–67.
- [30] S. Schottler, G. Becker, S. Winzen, Protein adsorption is required for stealth effect of poly(ethylene glycol)- and poly(phosphoester)-coated nanocarriers, *Nat. Nanotechnol.* 11 (4) (2016) 372–377.
- [31] A. Bateman, M.-J. Martin, S. Orchard, M. Magrane, S. Ahmad, E. Alpi, E.H. Bowler-Barnett, R. Britto, H. Bye-A-Jee, A. Cukura, P. Denny, T. Dogan, T. Ebenezer, J. Fan, P. Garmiri, L.J. da Costa Gonzales, E. Hatton-Ellis, A. Hussein, A. Ignatchenko, J. Zhang, UniProt: the Universal protein Knowledgebase in 2023, *Nucleic Acids Res.* 51 (D1) (2023) D523–D531, <https://doi.org/10.1093/nar/gkac1052>.
- [32] F. Sievers, D.G. Higgins, Clustal Omega, accurate alignment of very large numbers of sequences. https://doi.org/10.1007/978-1-62703-646-7_6, 2014.
- [33] T.A. Binkowski, CASTp: Computed Atlas of surface Topography of proteins, *Nucleic Acids Res.* 31 (13) (2003) 3352–3355, <https://doi.org/10.1093/nar/gkg512>.
- [34] A. Magnin, E. Pollet, V. Phalip, L. Avéroux, Evaluation of biological degradation of polyurethanes, *Biotechnol. Adv.* 39 (2020) 107457, <https://doi.org/10.1016/j.biotechadv.2019.107457>.
- [35] J.B. Procter, G.M. Carstairs, B. Soares, K. Mourão, T.C. Ofoegbu, D. Barton, L. Lui, A. Menard, N. Sherstnev, D. Roldan-Martinez, S. Duce, D.M.A. Martin, G. J. Barton, Alignment of Biological Sequences with Jalview, 2021, pp. 203–224, https://doi.org/10.1007/978-1-0716-1036-7_13.
- [36] I. Massova, P.A. Kollman, Computational alanine scanning to Probe Protein–Protein interactions: a novel approach to evaluate binding free energies, *J. Am. Chem. Soc.* 121 (36) (1999) 8133–8143, <https://doi.org/10.1021/ja990935j>.
- [37] V.B. Tsvetkov, A.V. Serbin, A novel view of modelling interactions between synthetic and biological polymers via docking, *Journal of Computer Aided Molecular Design* 26 (2012) 1369–1388, <https://doi.org/10.1007/s10822-012-9621-7>.
- [38] S. Miyamoto, P.A. Kollman, SETTLE: an analytical version of the SHAKE and RATTLE algorithm for rigid water models, *J. Comput. Chem.* 13 (8) (1992) 952–962, <https://doi.org/10.1002/jcc.540130805>.
- [39] B. Hess, H. Bekker, H.J.C. Berendsen, J.G.E.M. Fraaije, LINCS: a linear constraint solver for molecular simulations, *J. Comput. Chem.* 18 (12) (1997) 1463–1472, <https://doi.org/10.1002/jcc.540181209>.
- [40] G. Bussi, D. Donadio, M. Parrinello, Canonical sampling through velocity rescaling, *J. Chem. Phys.* 126 (1) (2007), <https://doi.org/10.1063/1.2408420>.
- [41] M. Parrinello, A. Rahman, Polymorphic transitions in single crystals: a new molecular dynamics method, *J. Appl. Phys.* 52 (12) (1981) 7182–7190, <https://doi.org/10.1063/1.328693>.
- [42] L.S. Doddia, I. Cabeza de Vaca, J. Tirado-Rives, W.L. Jorgensen, LigParGen web server: an automatic OPLS-AA parameter generator for organic ligands, *Nucleic Acids Res.* 45 (W1) (2017) W331–W336, <https://doi.org/10.1093/nar/gkx312>.
- [43] Z. Kurkcuoglu, P.I. Koukos, N. Citro, M.E. Trellet, J.P.G.L.M. Rodrigues, I.S. Moreira, J. Roel-Touris, A.S.J. Melquiond, C. Geng, J. Schaarschmidt, L.C. Xue, A. Vangone, A.M.J.J. Bonvin, Performance of HADDOCK and a simple contact-based protein-ligand binding affinity predictor in the D3R Grand Challenge 2, *J. Comput. Aided Mol. Des.* 32 (1) (2018) 175–185, <https://doi.org/10.1007/s10822-017-0049-y>.
- [44] A. Vangone, J. Schaarschmidt, P. Koukos, C. Geng, N. Citro, M.E. Trellet, L.C. Xue, A.M.J.J. Bonvin, Large-scale prediction of binding affinity in protein–small ligand complexes: the PRODIGY-LIG web server, *Bioinformatics* 35 (9) (2019) 1585–1587, <https://doi.org/10.1093/bioinformatics/bty816>.
- [45] G.D. Barone, D. Ferizović, A. Biundo, P. Lindblad, Hints at the Applicability of Microalgae and Cyanobacteria for the biodegradation of plastics, *Sustainability* 12 (24) (2020) 10449, <https://doi.org/10.3390/su122410449>.
- [46] T. Fecker, P. Galaz-Davison, F. Engelberger, Y. Narui, M. Sotomayor, L.P. Parra, C.A. Ramírez-Sarmiento, Active site flexibility as a Hallmark for efficient PET degradation by I. Sakaiensis PETase, *Biophys. J.* 114 (6) (2018) 1302–1312, <https://doi.org/10.1016/j.bpj.2018.02.005>.
- [47] T. Kang, J. Lin, L. Yang, M. Wu, Expression, isolation, and identification of an ethanol-resistant ethyl carbamate-degrading amidase from *Agrobacterium tumefaciens* d3, *J. Biosci. Bioeng.* 132 (3) (2021) 220–225, <https://doi.org/10.1016/j.jbiosc.2021.05.003>.
- [48] Y. Miki, F.R. Calviño, R. Pogni, S. Giansanti, F.J. Ruiz-Dueñas, M.J. Martínez, R. Basosi, A. Romero, A.T. Martínez, Crystallographic, Kinetic, and Spectroscopic study of the first Ligninolytic peroxidase presenting a catalytic Tyrosine, *J. Biol. Chem.* 286 (17) (2011) 15525–15534, <https://doi.org/10.1074/jbc.M111.220996>.
- [49] K. Piontek, E. Strittmatter, R. Ullrich, G. Gröbe, M.J. Pecyna, M. Kluge, K. Scheibner, M. Hofrichter, D.A. Plattner, Structural Basis of substrate Conversion in a new Aromatic Peroxygenase, *J. Biol. Chem.* 288 (48) (2013) 34767–34776, <https://doi.org/10.1074/jbc.M113.514521>.
- [50] Å.M. Ronkvist, W. Xie, W. Lu, R.A. Gross, Cutinase-catalyzed hydrolysis of poly(ethylene terephthalate), *Macromolecules* 42 (14) (2009) 5128–5138, <https://doi.org/10.1021/ma9005318>.
- [51] C. Roth, R. Wei, T. Oeser, J. Then, C. Föllner, W. Zimmermann, N. Sträter, Structural and functional studies on a thermostable polyethylene terephthalate degrading hydrolase from *Thermobifida fusca*, *Appl. Microbiol. Biotechnol.* 98 (18) (2014) 7815–7823, <https://doi.org/10.1007/s00253-014-5672-0>.
- [52] E. Santacruz-Juárez, R.E. Buendía-Corona, R.E. Ramírez, C. Sánchez, Fungal enzymes for the degradation of polyethylene: molecular docking simulation and biodegradation pathway proposal, *J. Hazard Mater.* 411 (2021) 125118, <https://doi.org/10.1016/j.jhazmat.2021.125118>.
- [53] J. Schmidt, R. Wei, T. Oeser, L. Dedavid e Silva, D. Breite, A. Schulze, W. Zimmermann, Degradation of polyester polyurethane by bacterial polyester hydrolases, *Polymers* 9 (12) (2017) 65, <https://doi.org/10.3390/polym9020065>.
- [54] M. Srikanth, T.S.R.S. Sandeep, K. Sucharitha, S. Godi, Biodegradation of plastic polymers by fungi: a brief review, *Bioresources and Bioprocessing* 9 (1) (2022) 42, <https://doi.org/10.1186/s40643-022-00532-4>.
- [55] M. Sundaramoorthy, M.H. Gold, T.L. Poulos, Ultrahigh (0.93 Å) resolution structure of manganese peroxidase from *Phanerochaete chrysosporium*: Implications for the catalytic mechanism, *J. Inorg. Biochem.* 104 (6) (2010) 683–690, <https://doi.org/10.1016/j.jinorgbio.2010.02.011>.
- [56] R. Wei, T. Oeser, J. Then, N. Kühn, M. Barth, J. Schmidt, W. Zimmermann, Functional characterization and structural modeling of synthetic polyester-degrading hydrolases from *Thermomonospora curvata*, *Amb. Express* 4 (1) (2014) 44, <https://doi.org/10.1186/s13568-014-0044-9>.
- [57] R.A. Wilkes, L. Aristilde, Degradation and metabolism of synthetic plastics and associated products by *Pseudomonas* sp.: capabilities and challenges, *J. Appl. Microbiol.* 123 (3) (2017) 582–593, <https://doi.org/10.1111/jam.13472>.
- [58] Z. Zhang, H. Peng, D. Yang, G. Zhang, J. Zhang, F. Ju, Polyvinyl chloride degradation by a bacterium isolated from the gut of insect larvae, *Nat. Commun.* 13 (1) (2022) 5360, <https://doi.org/10.1038/s41467-022-32903-y>.
- [59] A. Fazli, D. Rodriguez, Waste rubber recycling: a review on the evolution and properties of Thermoplastic Elastomers, *Materials* 13 (3) (2020) 782, <https://doi.org/10.3390/ma13030782>.
- [60] M.C. Feitor, C. Alves Junior, C.M. Bezerra, R. R. M. de Sousa, T.H. de C. Costa, Evaluation of aging in Air of poly (ethylene Terephthalat) in oxygen plasma, *Mater. Res.* 18 (5) (2015) 891–896, <https://doi.org/10.1590/1516-1439.305814>.
- [61] N. Flores-Castañón, S. Sarkar, A. Banerjee, Structural, functional, and molecular docking analyses of microbial cutinase enzymes against polyurethane monomers, *Journal of Hazardous Materials Letters* 3 (2022) 100063.
- [62] I. Aier, P.K. Varadwaj, U. Raj, Structural insights into conformational stability of both wild-type and mutant EZH2 receptor, *Sci. Rep.* 6 (1) (2016) 34984, <https://doi.org/10.1038/srep34984>.
- [63] Y. Zhao, C. Zeng, M.A. Massiah, Molecular dynamics simulation reveals insights into the mechanism of Unfolding by the A130T/V mutations within the MID1 Zinc-binding Bbox1 Domain, *PLoS One* 10 (4) (2015) e0124377, <https://doi.org/10.1371/journal.pone.0124377>.

- [64] B. Kamaraj, R. Purohit, *In silico* screening and molecular dynamics simulation of Disease-associated nsSNP in TYRP1 Gene and its structural Consequences in OCA3, BioMed Res. Int. 2013 (2013) 1–13, <https://doi.org/10.1155/2013/697051>.
- [65] K. Nagasubramanian, S. Jha, A.S. Rathore, K. Gupta, Identification of small molecule modulators of class II transactivator-I using computational approaches, J. Biomol. Struct. Dyn. 41 (17) (2023) 8349–8361, <https://doi.org/10.1080/07391102.2022.2133011>.
- [66] F. Sittel, A. Jain, G. Stock, Principal component analysis of molecular dynamics: on the use of Cartesian vs. internal coordinates, J. Chem. Phys. 141 (1) (2014), <https://doi.org/10.1063/1.4885338>.
- [67] A.M. Londhe, C.G. Gadhe, S.M. Lim, A.N. Pae, Investigation of molecular details of Keap1-Nrf2 inhibitors using molecular dynamics and Umbrella sampling techniques, Molecules 24 (22) (2019) 4085, <https://doi.org/10.3390/molecules24224085>.
- [68] S. Genheden, U. Ryde, The MM/PBSA and MM/GBSA methods to estimate ligand-binding affinities, Expert Opin. Drug Discov. 10 (5) (2015) 449–461, <https://doi.org/10.1517/17460441.2015.1032936>.
- [69] S.K. G, K. N, E. Elumalai, K.K. Gupta, Identification of CXCR4 inhibitors as a key therapeutic small molecule in renal fibrosis, J. Biomol. Struct. Dyn. 42 (16) (2023) 8441–8453, <https://doi.org/10.1080/07391102.2023.2246575>.
- [70] R.K. Rizqillah, J.F. Fatriansyah, Sulhadi Fadilah, S. Wahyuni, M.A. Sudirman, H.C. Nafisah, S.D. Lestari, In silico molecular docking and molecular dynamics examination of Andrographis paniculata compounds of Andrographolide, Neoandrographolide, and 5-hydroxy-7,8,2',3'-tetramethoxyflavone inhibition activity to SARS-CoV-2 main protease, BIO Web of Conferences 41 (2021) 07002, <https://doi.org/10.1051/bioconf/20214107002>.
- [71] S. Chen, L. Su, S. Billig, W. Zimmermann, J. Chen, J. Wu, Biochemical characterization of the cutinases from Thermobifida fusca, J. Mol. Catal. B Enzym. 63 (3–4) (2010) 121–127, <https://doi.org/10.1016/j.molcatb.2010.01.001>.
- [72] A.K. Urbanek, K.E. Kosiorowska, A.M. Mirończuk, Current Knowledge on polyethylene terephthalate degradation by Genetically modified microorganisms, Front. Bioeng. Biotechnol. 9 (2021), <https://doi.org/10.3389/fbioe.2021.771133>.
- [73] X. Qi, W. Yan, Z. Cao, M. Ding, Y. Yuan, Current Advances in the biodegradation and Bioconversion of polyethylene terephthalate, Microorganisms 10 (1) (2021) 39, <https://doi.org/10.3390/microorganisms10010039>.
- [74] J. Qiu, Y. Chen, L. Zhang, J. Wu, X. Zeng, X. Shi, L. Liu, J. Chen, A comprehensive review on enzymatic biodegradation of polyethylene terephthalate, Environ. Res. 240 (2024) 117427, <https://doi.org/10.1016/j.envres.2023.117427>.
- [75] H. Yuan, J. Wu, X. Wang, J. Chen, Y. Zhong, Q. Huang, P. Nan, Computational identification of amino-acid mutations that further improve the activity of a Chalcone-Flavonone Isomerase from Glycine max, Front. Plant Sci. 8 (2017), <https://doi.org/10.3389/fpls.2017.00248>.
- [76] A. Subramani, C.A. Floudas, Structure prediction of loops with fixed and flexible Stems, J. Phys. Chem. B 116 (23) (2012) 6670–6682, <https://doi.org/10.1021/jp2113957>.
- [77] D. Chen, N. Oezguen, P. Urvil, C. Ferguson, S.M. Dann, T.C. Savidge, Regulation of protein-ligand binding affinity by hydrogen bond pairing, Sci. Adv. 2 (3) (2016), <https://doi.org/10.1126/sciadv.1501240>.
- [78] C.C. David, D.J. Jacobs, Principal component analysis: a method for determining the essential dynamics of proteins. https://doi.org/10.1007/978-1-62703-658-0_11, 2014.